CONVECTION IN A DIFFERENTIALLY HEATED ROTATING SPHERICAL SHELL OF BOUSSINESQ FLUID WITH RADIATIVE FORCING

By

David Babalola

Faculty of Science, University of Ontario Institute of Technology

December 21, 2012

A thesis submitted to the
University of Ontario Institute of Technology
in accordance with the requirements of the degree
of Master of Science in the Faculty of Science

Abstract

In this study we investigate the flow of a Boussinesq fluid contained in a rotating, differentially heated spherical shell. Previous work, on the spherical shell of Boussinesq fluid, differentially heated the shell by prescribing temperature on the inner boundary of the shell, setting the temperature deviation from the reference temperature to vary proportionally with $-\cos 2\theta$, from the equator to the pole. We change the model to include an energy balance equation at the earth's surface, which incorporates latitudinal solar radiation distribution and ice-albedo feedback mechanism with moving ice boundary. For the fluid velocity, on the inner boundary, two conditions are considered: stress-free and no-slip. However, the model under consideration contains only simple representations of a small number of climate variables and thus is not a climate model per se but rather a tool to aid in understanding how changes in these variables may affect our planet's climate.

The solution of the model is followed as the differential heating is changed, using the pseudo arc-length continuation method, which is a reliable method that can successfully follow a solution curve even at a turning point.

Our main result is in regards to hysteresis phenomenon that is associated with transition from one to multiple convective cells, in a differentially heated, co-rotating spherical shell. In particular, we find that hysteresis can be observed without transition from one to multiple convective cells. Another important observation is that the transition to multiple convective cells is significantly suppressed altogether, in the case of stress-free boundary conditions on the fluid velocity. Also, the results of this study will be related to our present-day climate.

Acknowledgements

All glory be to God Almighty, who has made everything beautiful in His own time.

Many thanks to my supervisors, Profs. Greg Lewis and Bill Langford, for their great help and unalloyed supports throughout the duration of my studies at the University of Ontario Institute of Technology. You guys are great!.

I would also like to thank Engineer Christopher Babalola and his family who have encouraged and supported me all along both with finances and prayers to make the journey much easier. A million thanks to you. I must not forget to mention the enormous assistance of Pastor Victor Erhabor and his family who have always been there for me. May God be with you. My friends - Carla Lawrence, Tolulope Fadina, and my parents - Mr and Mrs Babalola, thanks for your supports in different ways.

To all the staff and faculty at UOIT, who have provided me with an excellent atmosphere for learning, I say thank you.

Author's Declaration

I declare that this work was carried out in accordance with the regulations of the University of Ontario Institute of Technology. The work is original except where indicated by special reference in the text and no part of this document has been submitted for any other degree. Any views expressed in the dissertation are those of the author and in no way represent those of the University of Ontario Institute of Technology. This document has not been presented to any other University for examination either in Canada or overseas.

David Babalola

Date: December 21, 2012

Contents

List of Figures

List of Tables

Chapter 1
Introduction

1.1 Background

1.1.1 The Climate System

The *climate system* can be defined as a composite system consisting of five major interactive components: the atmosphere, the hydrosphere with the oceans, the cryosphere, the lithosphere, and the biosphere [18]. The biosphere is the whole body of ecosystems that comprises living organisms such as plants, animals and microbes, and their non-living environment. The hydrosphere refers to all the waters of the earth, including the rivers and the oceans. The lithosphere, sometimes called the geosphere, is the solid parts of the earth. The cryosphere is the collective iced parts of the climate system. It includes ice caps, ice sheets, glaciers and snow covers.

The atmosphere is made up of a gaseous mixture, almost evenly distributed over the earth's surface. In terms of dimension, it is primarily contained within 100 km in the vertical direction and of the order of 20 000 km measured from north pole to south pole [20] in the horizontal. The atmosphere consists of several layers consisting of different composition, temperature and atmospheric pressure (that decreases with height). The layers are called the troposphere, the stratosphere, the mesosphere, and the thermosphere; between every two layers is an idealized separation, called a *pause*. For example the tropopause separates the troposphere from the stratosphere. The composition of the atmosphere consists of gases, such as nitrogen, oxygen, and other inert gases and suspensions such as liquid, clouds, dust particles, sulfate aerosols and volcanic ash. The concentrations of these atmospheric elements can vary from layer to layer in time and space.

The components of the climate system are open to each other, and thus interact

with one another as a result of their non-isolation. They have different structures, composition, physical properties and thermodynamic behaviors. They are also open to receive energy from the solar system but can not transfer or exchange matter with outer space. A subsystem or group of subsystems with similar but not necessarily identical behaviors can be classified as an *internal system* while other subsystems that are not internal are called *external systems*. For example, the atmosphere can be considered as a subsystem or internal system of the climate system and other subsystems such as geosphere, biosphere, etc., can be considered as external systems. As a result of this classification of the global climatic system that is very complex due to the nonlinear interactions of the adjoint components, it is possible to study the dynamics of a subsystem separate from the other systems.

1.1.2 Current Issues in Climate Change

Climate change has become an important issue facing our planet and our future. The term *climate change* has been defined in various manners. According to the Intergovernmental Panel on Climate Change, climate change refers to a change in the state of the climate that can be identified (e.g. using statistical tests) by changes in the mean and/or the variability of its properties, and that persists for an extended period, typically decades or longer. It refers to any change in climate over time, whether due to natural variability or as a result of human activity [18].

Alternatively, the United Nations Framework Convention on Climate Change refers to climate change as a change of climate which is attributed directly or indirectly to human activity that alters the composition of the global atmosphere and which is, in addition to natural climate variability, observed over comparable time periods [15].

The consequences of climate change, in particular those due to increases in green house gases (GHG) in the atmosphere, certainly affect our lives. Some of the obvious consequences are increased annual mean temperature, increased number of glacier lakes, increased ground instability in permafrost regions, increased sea levels, warming of lakes and rivers in some regions which affects water quality, and excess heat-related

mortality in some parts of the world. It has been observed that global GHG emissions will continue to grow over the next couple of decades [18]. The immediate effect of the rise in GHG emissions is that the outgoing infrared radiation is trapped in the atmosphere, and as a result there is an increase in the annual mean temperature of the earth. Consequently the ice at the poles may melt and flow into the sea, therefore increasing the sea level. Also, beyond the 21^{st} century, anthropogenic (i.e. human-induced) warming and sea level rise may continue for centuries, even if GHG concentrations were to be stabilized. This is due to the delay associated with climate processes and feedbacks, in particular, due to the long time it takes to transport heat into deep ocean. That means the consequences of climate change will stay with us for years to come.

1.1.3 Major Climate Influences

Radiation

Solar radiation is the primary energy source for the earth. The incoming solar radiation is subject to absorption, scattering and reflection by various gases of the atmosphere. The remainder of the solar radiation that reaches the earth's surface is absorbed by the other climatic system components (e.g. hydrosphere, geosphere, cryosphere and biosphere). The amount of solar energy reaching the earth's surface varies from place to place, depending on how transparent the atmosphere is, and on the angle of incidence of the radiation. The energy, so absorbed, is either converted to internal or heat energy, which acts to raise the temperature of the planet as a whole, or is transformed to potential or kinetic energy to do work against the surrounding environment.

Albedo is the ratio of reflected to incident solar radiation, and the *solar constant* is the amount of incoming solar electromagnetic radiation per unit area that would be incident on a plane perpendicular to the sun's rays, at a distance of one astronomical unit (AU) (roughly the mean distance from the sun to the earth). However, according to Prevost's principle of the late 18th century: all bodies with a temperature above 0K emit energy whose quality (in terms of frequency) depends on their temperature.

This is consistent with Stefan-Boltzmann's law: the energy radiated by a blackbody radiator per second per unit area is proportional to the fourth power of the absolute temperature; it is also consistent with Wien's displacement law: for blackbody radiation the wavelength of maximum emission is inversely proportional to the absolute temperature [20]. From the definitions, it shows that the amount of emitted energy is a function of the temperature of the emitting body. The larger the amount of emitted energy, the shorter the wavelength of its peak. In the electromagnetic spectrum, the solar energy that drives the climatic system is in the range of $0.1 - 2.0\mu m$, i.e. in the ultraviolet, visible, and infrared regions; while most of the outgoing terrestrial radiation to outer space is in the range of $4.0 - 60\mu m$, i.e. in the infrared range. Radiation is defined as short wave when its wavelength $\lambda < 4.0\mu m$, and long wave when its wavelength $\lambda \geq 4.0\mu m$. The outgoing energy, emitted by the earth's surface and atmosphere, is long-wave. Ultimately, some of this long-wave radiation escapes to outer space, but some is absorbed as it travels through the atmosphere. When the energy of the incoming radiation balances that of the outgoing radiation, an equilibrium is obtained. This is referred to as *energy balance*, and it is this balance that keeps the earth in its long-term perpetual state of quasi-equilibrium. Sellers states that, if all other variables are held constant, a decrease in the solar constant by about 2% would be sufficient to create another ice age, with ice caps extending equatorward to 50^0 latitude, and an increase in the solar constant of about 3% would probably be sufficient to melt the ice sheets [22]. How solar radiation and the solar constant affect the energy balance is detailed in Section 2.1.

Clouds

Clouds are visible in the atmosphere. A cloud is a mass of liquid droplets, or frozen crystals made of water or various chemicals, suspended in the atmosphere above the earth's surface. The majority of the earth's cloud is in the troposphere. It has an influence on the energy balance, because it reflects solar radiation back to outer space, thus increasing the albedo, and is opaque to infrared radiation. Infrared radiation

that is blocked by the cloud from exiting the atmosphere increases the annual mean temperature of the earth. The net effect of these two competing characteristics of the cloud contributes to the radiative forcing of the climate.

Green House Gases

Greenhouse gases (GHG) are defined as those gaseous constituents of the atmosphere, both natural and anthropogenic, that absorb and re-emit infrared radiation. There are three constituents of the atmosphere that are the most important greenhouse gases: carbon dioxide (CO_2), water vapor, and methane (CH_4). They are accountable for most of the absorption of infrared radiation in the atmosphere. They allow easy passage of solar radiation but block the escape of long-wave infrared radiation. By their nature, the greenhouse gases are invisible in the atmosphere [15]. Pierrehumbert states that there are two categories of greenhouse gases; *long-lived greenhouse gases* and *short-lived greenhouse gases* [21]. An example of a long-lived greenhouse gas is CO_2, while water vapor is an example of a short-lived greenhouse gas. It takes from several decades to a thousand years to remove long-lived greenhouse gases from the atmosphere, because of their chemical stability and long-term influence on the climate; but it takes only weeks to years to remove short-lived greenhouse gases by condensation or rapid chemical reactions. The primary importance of short-lived greenhouse gases is as a feedback mechanism, either to amplify or offset changes due to other factors including the long-lived greenhouse gases.

Many of the greenhouse gases occur naturally, but the present increase in the atmospheric concentrations of GHGs is due mostly to human industrial activities. These activities include agricultural practices that produce methane gas when bacteria break down organic matters, fossil fuels that increase CO_2 concentrations in the atmosphere when they are burnt, and deforestation that reduces the number of trees that partake in photosynthetic process. Greenhouse gases play a significant or dominant role in radiative forcing of the climate.

1.1.4 Atmospheric Circulation

The long journey to a better understanding of atmospheric circulation began with the Hadley Principle proposed by George Hadley, in his paper of 1735: Concerning the Cause of the General Trade Winds [7]. The trade winds can be defined as the predominant circulation pattern of easterly winds, found in the tropics, in the lower part of the troposphere, near the earth's equator. The trade winds blow from the northeast in the northern hemisphere and from the southeast in the southern hemisphere. Hadley explained that atmospheric circulation is a result of the relative motion between the motions of the earth and of the air. By atmospheric circulation, we mean large-scale air movement, by means of which heat energy is distributed on the earth's surface. For instance, given the spherical shape of the earth's surface and the linear relationship between velocity and distance from the axis of rotation, if the air in the tropics of the northern hemisphere has lesser velocity than that of the air at the equator, and moves from the tropics towards the equator, it will have a relative motion contrary to that of the daily motion at the equator, and a northeast wind will be produced. Similarly, if air in the tropics with lesser velocity than that of the air at the equator (in the southern hemisphere), moves from tropics towards the equator, it will have a relative motion contrary to that of the daily motion at the equator, and a southeast wind will be produced. Similar relevant ideas were put forward by Edmond Halley, who stated that the deviation of trade winds from straight east was due to the meridional flow of dense air toward the latitude of maximal radiative heating [8, 2], and Robert Hooke who invoked the centrifugal force of the earth's rotation to explain the equator-ward component of trade winds [2]. From the above ideas, it is obvious that differential heating coupled with the earth's rotation causes the atmospheric circulations and gives directions to the winds. The major effect of the earth's rotation on atmospheric motion is due to what is referred to today as the *Coriolis effect*.

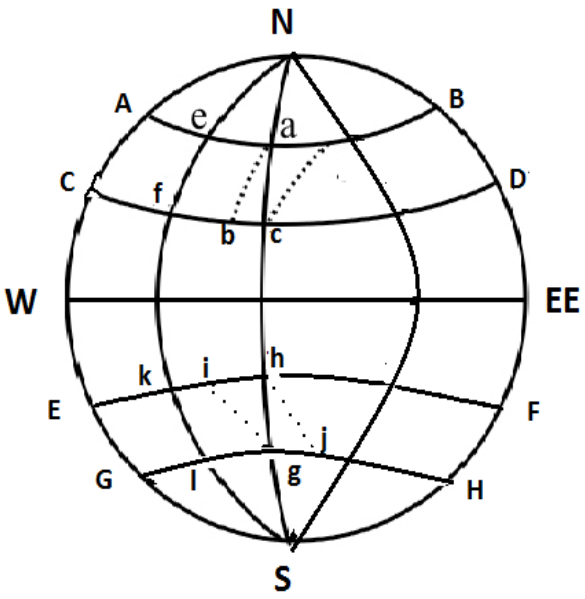

Figure 1.1: Graphical reconstruction of the deflective effect of the earth's rotation

Coriolis Effect

The Coriolis force is of great importance because we are studying the dynamics of the atmosphere in a non-inertial frame of reference. In a rotating reference frame, a moving object tends to experience deflection; this is called the Coriolis effect. The earth rotates about its axis, and the direction of rotation is counter-clockwise if viewed from the north pole and clockwise if view from the south pole. In a counter-clockwise rotating reference frame, the deflection of the moving body is to the right of its direction of motion, and in a clockwise rotating reference frame, the deflection of the moving body is to the left of its direction of motion. In a nutshell, an object traveling on the rotating earth will get pulled to its right in the northern hemisphere, while in the southern hemisphere, the object gets pulled to its left. A graphical illustration of the Coriolis effect is shown in Figure 1.1, and presented below in the spirit of [2]. Let **N** and **S** be North and South poles respectively, **W** to **EE** be the equatorial circle. Two latitudes are marked **AB** and **CD** in the northern hemisphere, **EF** and **GH** in the southern hemisphere, and the remaining are meridians.

Two directions are of importance here. The direction of the rotation of the earth and the direction of the translational motion of the air. Suppose that the air at **a** is

only under the influence of the rotational motion of the earth (i.e. it is stationary with respect to the earth), then in 12 hours it will cover half of what the latitude circle **AB** covers from west to east (in 24 hours coming back to where it started). Now assume that the air in **a** is moving to **c** along a meridian, and the north wind is following the curve **ea** from west to east due to rotation of the earth. Provided there are no obstacles that could meet the air during its course, the air on the moving earth would not be at **c**, but at **b** at the end of its journey. The time it takes for the earth at latitude **CD** to cover **fc** from west to east is the same time it takes the earth at latitude **AB** to cover **ea**, and at the end of this time, the air from **a** will find itself at **b**.

It does not matter whether the earth's motion lags behind that of the air or the air's motion lags behind that of the earth, a combined movement of both earth and air will follow along a certain diagonal curve **ab**, of which the sides **ac**, **bc** and **ab** represent those of northerly wind velocity, the difference of the motion at both latitude circles, and the north-westerly wind velocity, respectively. The same reasoning applies to the motion of air moving in any direction of the earth. The Coriolis effect becomes pronounced only for motions occurring over large distances and long periods of time, such as large-scale movement of air in the atmosphere or water in the ocean.

Also, complementing the Coriolis effect is the centrifugal force. The Coriolis force is proportional to the rotation rate and the centrifugal force is proportional to its square. The centrifugal force acts outwards in the radial direction and is proportional to the distance of the body from the axis of the rotating frame. The Coriolis effect is higher at the poles than at the equator. The Coriolis force is only one of many forces; the circulation patterns that are observed in the atmosphere actually result from a balance of many factors, e.g. pressure gradients, the centrifugal force, the Coriolis force and the frictional force.

Hadley Cells

The Hadley cell is one of the three cells that make up the general atmospheric circulations in each hemisphere. The other two are the Ferrel cell in the mid-latitudes

and the Polar cell in the high latitudes as shown in Figure 1.2. The Hadley cell is the most persistent of all the three cells. It is bounded roughly by 30^0, north and south of the equator. The motion of the atmospheric circulation is a combined zonal (i.e. east-west) and meridional (i.e. along a meridian) mass transport. It is characterized by mass transport towards the equator (by the prevailing north-east trade wind in the northern hemisphere and south-east trade wind in the southern hemisphere) in the lower troposphere, with rising motion near the equator, sinking motion in the subtropics, and mass transport towards the pole in the upper troposphere.

Due to the differential heating induced by the solar radiation, the air at the equator is warm and at low pressure, while the air at the poles is cold and at high pressure. The warm, low pressure air at the equator rises, loses heat and moves toward the high pressure region at the poles. As it approaches the poles and loses more heat, the air sinks into the region of high pressure, from which the cold air has moved to occupy the space the warm, low pressure rising air at the equator has left, and a convection cell is formed.

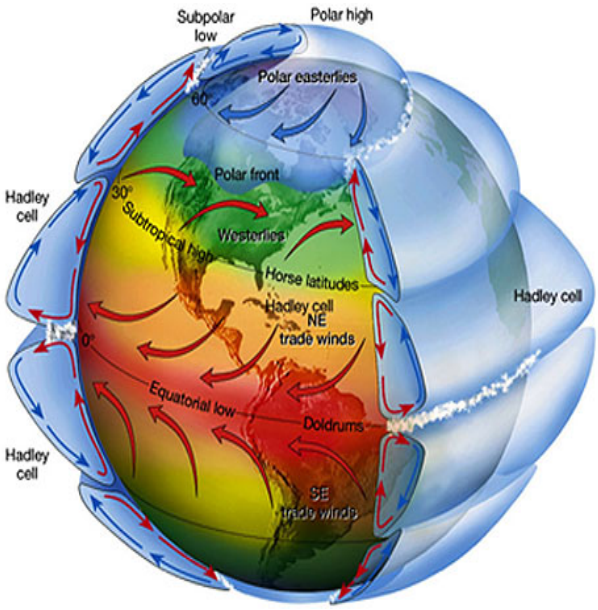

Figure 1.2: The atmospheric circulation showing three cells: the Hadley cell at the equatorial region, the Polar cell at the polar region and the Ferrel cell in between the Hadley and the Polar cells. (The picture is originally uploaded on http://serc.carleton.edu/earthlabs/climate/5.html)

Current discussions on climate have raised the issue of poleward expansion of Hadley cells. This expansion has been attributed to global warming of the atmosphere [12]. Langford and Lewis use a variant of the model presented here to observe poleward expansion in the Hadley cell, with some weakening in the velocity of atmospheric circulation [10].

1.2 Relationship with Other Works

A mathematical model of convection of a Boussinesq fluid in a rotating spherical shell is considered and analyzed using numerical computations, guided by bifurcation theory in [11, 10]. Also in [10] the model is nondimensionalized (i.e. the variables in the model are put in dimensionless form). Here, however, we follow [11]. Hence, nondimensionalization of variables is not considered in this work; whenever there is need for reference to dimensionless parameters such as the Prandtl number, we refer to [10]. The boundary conditions imposed on the fluid velocity in [10], are no-slip and stress-free at the inner surface and outer surface respectively, while [11] uses no-slip boundary conditions at the inner and outer surfaces. In this thesis, both no-slip and stress-free conditions are considered at the inner boundary. In one case, no-slip boundary conditions are imposed on the fluid velocity along the inner surface of the spherical shell, and stress-free boundary conditions are imposed on the velocity on its outer surface. In the other case, stress-free boundary conditions are imposed on both the inner and outer surfaces of the spherical shell. Other properties, such as the rotation rate, the gap width between the concentric spherical shells, and the radius of the inner shell, are taken to be the same as those of [11, 10].

In [11, 10], the heat transfer mechanism is included implicitly as a function of the temperature gradient ΔT and $-\cos 2\theta$ between the pole and the equator, where θ is the polar angle. The differential heating is maximum at the equator ($\theta = \frac{\pi}{2}$) and minimum at the poles ($\theta = 0, \pi$). Recent works on climate change are inclined to a radiative forcing mechanism that is determined by energy balance, and thus, in order to have a more realistic model, we included this in our equations. The radiative forcing includes the energy balance equation of the earth-atmosphere system, where the earth's average

temperature is allowed to depend on solar radiation [4, 22, 17]. For our model, there is a linear relationship between solar radiation and differential heating. In order to see the influence of the radiation variation (or differential heating) on the temperature at each latitude, we take the solar distribution to be longitudinally averaged, i.e. we allow the solar distribution to vary with latitude only [4]. The amount of latitudinal solar absorption will also be influenced by albedo. The latitudes that are covered with an ice sheet will receive a lower amount of solar energy (due to higher reflection by ice) than the latitudes that are ice-free [4, 17].

Convection in a rotating spherical shell has been extensively studied with different forms of forcing and boundary conditions. For example, the thermal convection of Boussinesq fluid in a moderately rotating spherical shell is studied in [9]; in particular the fluid is forced by a uniform heat source, and the solutions are characterized by rotation rate. Zhang *et al.* [23] also study convection in a rapidly rotating sphere, in which the convection is analyzed using an asymptotic method. They consider the influence of stress-free boundary conditions on convection in a Boussinesq fluid with small Prandtl number. The convection in rotating spherical shells of Boussinesq fluid studied, by Net *et al.* [16], considers forcing by external compositional and temperature gradients. The temperature gradient included in their model is in the form of differential and internal heating. In fact, they critically examine the influence of the mixture of two fluids on the onset of convection, induced by the two types of forcing. All these studies use a dynamical system's approach to study the flow transitions. This is the philosophy we shall follow.

The linear stability analysis of the convection of a Boussinesq fluid is carried out in [11], and the existence of cusp bifurcation in a differentially heated rotating spherical shell is also shown; therefore, we do not attempt to reproduce these results. With this in mind, much reference will be made to [11]. Also, Marcus *et al.* [13, 14] use two control parameters (i.e. the radius ratio and the Reynolds number) to isolate different forms of transitions. They opined that the nature of the transitions that occur in differentially rotating spheres, and their stabilities, depend largely on the system's radius ratio, and that there is a critical Reynolds number below which Taylor vortices

may not be virtually detected, and above which symmetrically arranged vortices can be found. The Taylor vortices are analogous to convective cells. Also, they observe that vortices never form in a spherical shell with a very large radius ratio. Though the model studied here differs significantly from the one in [13, 14], their study indicates that it will be challenging to obtain radius ratios and Reynolds numbers, for which there will be a visible transition to multiple convective cells, while simultaneously locating the bifurcation that is associated with it.

Despite all the works done on the convection of Boussinesq fluids in rotating spherical shells with different types of forcing and boundary conditions used, it is worthwhile to mention that this work is unique. Most do not consider a latitudinal variation of the heating, and this is the first time an energy balance equation is used to drive convection in a spherical shell of Boussinesq fluid.

1.3 Project Direction

It is extremely difficult to have a single model that includes all the climate subsystems due to their complexity in terms of their inter-relationships. Therefore, in our work, the hydrosphere, the lithosphere, the biosphere are ignored and only the atmosphere is considered. Also, within the atmospheric system, the troposphere is most important for this study. Though it is the thinnest layer of the atmosphere, it constitutes the majority of the mass of the atmosphere. Recall that in Section 1.1.3, we identified solar radiation, clouds and greenhouse gases as major climate influences. The collective effect of clouds and greenhouse gases is to alter the energy balance of the climate and they directly contribute to the increase in average temperature of the earth. Therefore, we assume their contributions can be considered as part of the differential heating of the system. The solar radiation is ultimately the source of the differential heating because the equator receives more of the heating than the poles.

We will develop two variants of the model studied in [11]. In both variants, the boundary condition of the temperature of the model in [11] is changed from a prescribed temperature on the inner boundary to a radiative forcing equation. Lewis and Langford found transition to multiple convective cells in [11], and attributed the tran-

sition to a cusp bifurcation. We investigate their claims by studying the two variants of our model. In one of the variants of the model, the inner boundary condition on the fluid velocity is changed to stress-free, while in the other variant no-slip conditions are imposed on the inner boundary. It is found that transition to multiple cells occurs only in a model with the no-slip boundary condition imposed at the inner boundary. For this case, we search for evidence of hysteresis. Also, an ice-albedo feedback mechanism with moving ice boundary is included in both variants of the model. It is possible to study the dynamics of the system with or without the ice-albedo feedback, by switching on and off the ice-albedo feedback mechanism.

The model under consideration is not a climate model per se. In particular, we consider the spherical shell to be at the laboratory scale, and we take the fluid to have the properties of water. Thus, we do not expect to obtain quantitatively accurate solutions, however, we do expect our simple model to exhibit the qualitative features of flows for which differential heating and rotation play an important role. Thus, we consider our model as a tool that may aid in developing a better understanding of how certain climate variables may affect our planet's climate.

Chapter 2

The Mathematical Model

2.1 Radiative Forcing

In this section, the various roles of the atmospheric constituents as they affect the amount of energy available for the dynamics of the atmosphere are considered. Mathematically, we proceed with the derivation of the energy-balance equation that will be used as the inner boundary equation for the model. The first law of thermodynamics gives the time evolution of the energy on the earth's surface as:

$$\frac{\partial T}{\partial t} = Q_s - I + S_A, \tag{2.1.1}$$

where Q_s is the meridional and radial energy transport, S_A is the solar absorption and I is the outgoing radiation. The outgoing radiation can be expressed in terms of its temperature empirically as in [4]:

$$I = A + BT - (A_1 - B_1 T)n, \tag{2.1.2}$$

where T is the temperature at the earth's surface in ${}^0C$; A, A_1, B, B_1 are empirical coefficients, and n is the cloudiness as a fraction of unity. For a cloudless atmosphere ($n = 0$), equation (2.1.2) coincides with the empirical formula used by North in [17]. The solar absorption S_A depends on the solar constant Q, the meridional (i.e. pole to equator) distribution of solar radiation $S(\theta)$, and the absorption coefficient a, which is a function of the albedo. Both the solar meridional distribution and the absorption coefficient vary with colatitude θ, where the colatitude is the complementary angle of the latitude, i.e. the difference between 90^0 and the latitude. The solar energy absorbed by the earth's surface has the form:

$$S_A = QS(\theta)a(\theta). \tag{2.1.3}$$

The solar meridional distribution $S(\theta) = \frac{1}{2}(1 - \cos 2\theta)$ is chosen so that its maximum is at the equator ($\theta = \frac{\pi}{2}$) and its minimum is at the pole ($\theta = 0$). By the mere fact that $S(\theta)$ is minimum and maximum at the pole and equator, respectively, this imposes a differential heating between the pole and the equator. The absorption coefficient is defined as $a = 1 - \beta(\theta)$ (see [4, 22, 17]), where β is the albedo which we assume is given by $\beta(\theta) = 0.62 - 0.3H_m(T, T_0)$, and H_m is the Hill function:

$$H_m(T, T_0) = \frac{T^m}{T_0^m + T^m}, \tag{2.1.4}$$

for which $H_m(0, T_0) = 0$, and $H_m(T, T_0)$ monotonically tends quickly to 1 as T increases from T_0, where T_0 is the temperature at which the ice boundary forms. The value of m is chosen reasonably large so that it is a smooth approximation of the step function as shown in Figure 2.1. The ice boundary is the latitude at which the surface temperature equals T_0, i.e. where the ice sheet stops. The ice-covered portion of the earth's surface has a higher value of albedo than the ice-free surface, hence, there is a jump in the values of the albedo across the boundary. This jump is modelled by the Hill function. That is, for portions of the surface for which $T < T_0$, the surface is ice-covered, $H_m \approx 0$ and the albedo $\beta = 0.62$. For $T > T_0$, no ice is present and $H_m \approx 1$ and we have the lower albedo $\beta = 0.32$. Thus, we have the energy absorbed at the surface as:

$$S_A = \frac{Q}{2}(1 - \beta(\theta))(1 - \cos 2\theta). \tag{2.1.5}$$

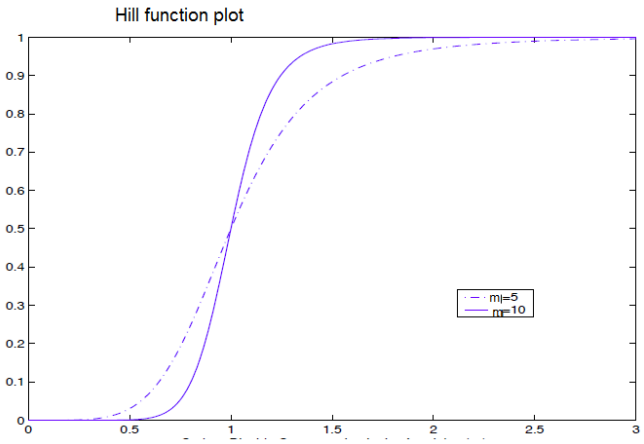

Figure 2.1: The plot of Hill function in equation 2.1.4, with $T_0 = 1$ and $m = 5, 10$.

For a given latitude, the absorbed energy is not always equal to the outgoing energy, the difference is absorbed by the atmosphere, which can set up temperature gradients. We model the resulting heat transport mechanism by:

$$Q_s = D_R\left(\frac{\partial^2}{\partial r^2}+\frac{2}{r}\frac{\partial}{\partial r}\right)T + D_H\left(\frac{1}{r^2}\frac{\partial^2}{\partial\theta^2}+\frac{\cos\theta}{r^2\sin\theta}\frac{\partial}{\partial\theta}\right)T, \tag{2.1.6}$$

where D_R is the diffusion coefficient in the vertical direction, D_H is the diffusion coefficient in the horizontal direction. The diffusion in the vertical describes the mechanism by which heat is exchanged between the surface and the overlying fluid. We substitute equations (2.1.2)–(2.1.6) into equation (2.1.1) to obtain a radiative forcing equation which is imposed on the inner surface as a boundary equation:

$$\begin{aligned}\frac{\partial T}{\partial t} &= D_R\left(\frac{\partial^2}{\partial r^2}+\frac{2}{r}\frac{\partial}{\partial r}\right)T + D_H\left(\frac{1}{r^2}\frac{\partial^2}{\partial\theta^2}+\frac{\cos\theta}{r^2\sin\theta}\frac{\partial}{\partial\theta}\right)T \\ &\quad -I(\theta)+QS(\theta)a(\theta),\end{aligned} \tag{2.1.7}$$

where we have ignored the effects of clouds ($n = 0$) in (2.1.2) on the incoming radiation, and I, D_R, D_H, Q, a and S are as defined above.

2.2 Model Equations

Although the portion of the atmosphere we are studying is the troposphere and the fluid is air, for this model, water is taken as the fluid, and the troposphere is represented by a confined space between two co-rotating shells called a *spherical shell*. The choice of studying the troposphere only is based on the fact that more than 99% of the atmospheric mass is found below an altitude of only 30 km within which tropopause is about 10 km [20], and the choice of water as the fluid is because water represents a simple, yet still realistic, fluid that can give the desired dynamics when it is heated. The model studied here is as presented in [11], with the exception of the radiative forcing at the inner boundary and stress-free conditions at the top boundary. Thus, the differential heating is imposed through the solar meridional distribution $S(\theta)$. In addition, we also make a comparison of the effects of using stress-free or no-slip boundary conditions on the velocity at the inner boundary.

The Navier-Stokes equations in the Boussinesq approximation are used to model

the fluid flow within the spherical shell. By the Boussinesq approximation, we mean all variations of fluid properties are considered to be negligible, except the density where it is multiplied by gravity. For our atmosphere, a warm fluid is less dense than a cold fluid, therefore we express the relationship between the density and temperature via the equation of state of the fluid as:

$$\rho = \rho_0 \left(1 - \alpha \left(T - T_r\right)\right), \tag{2.2.1}$$

where ρ is the density of the fluid, T is the temperature, α is the (constant) coefficient of thermal expansion and ρ_0 is the density at a reference temperature T_r. The quantity $\alpha\left(T - T_r\right)$ is dimensionless and assumed to be small.

The fluid (i.e. water) is contained within a spherical shell with inner sphere of radius r_a and outer sphere of radius r_b. The inner sphere represents the earth's surface, the outer shell represents the tropopause, and in between these concentric spheres is the troposphere.

The following are the model assumptions:

- gravity is assumed to act radially everywhere in the shell,
- the spherical shell rotates at rate Ω about the polar axis,
- the inner and outer spheres rotate at the same rate,
- there is rotational symmetry about the polar axis,
- there is reflectional symmetry about the equator.

The assumptions of rotational and reflectional symmetry are vital because they will reduce the domain of computation; as such, the solution we obtain on the reduced domain gives the full solution of the model when it is reflected across the equator and rotated around the polar axis.

The Navier-Stokes Boussinesq equations are partial differential equations that de-

scribe the time evolution of the vector fluid velocity and the temperature of the fluid:

$$\begin{aligned}\frac{\partial \mathbf{u}}{\partial t} &= \nu\nabla^2\mathbf{u} - 2\boldsymbol{\Omega}\times\mathbf{u} + [g\mathbf{e}_r + \boldsymbol{\Omega}\times(\boldsymbol{\Omega}\times\mathbf{r})]\,\alpha\,(T - T_r) \\ &\quad -\frac{1}{\rho_0}\nabla p - (\mathbf{u}\cdot\nabla)\,\mathbf{u}, \qquad (2.2.2)\\ \frac{\partial T}{\partial t} &= \kappa\nabla^2 T - (\mathbf{u}\cdot\nabla)\,T, \qquad (2.2.3)\\ &\quad \nabla\cdot\mathbf{u} = 0, \qquad (2.2.4)\end{aligned}$$

where $\mathbf{u} = \mathbf{u}(r,\theta,\varphi,t) = w\mathbf{e}_r + v\mathbf{e}_\theta + u\mathbf{e}_\varphi$ is the fluid velocity in vector form, u is the zonal fluid velocity (or azimuthal velocity), v is the polar fluid velocity (or meridional velocity), and w is the radial fluid velocity. The r, θ, φ are radial, polar and zonal spatial variables respectively, t is the time. The $\mathbf{e}_r$, $\mathbf{e}_\theta$, $\mathbf{e}_\varphi$ are unit vectors in the radial, polar and zonal directions respectively, $T = T(r,\theta,\varphi,t)$ is the temperature of the fluid, $\boldsymbol{\Omega} = \Omega\,(\cos\theta\mathbf{e}_r - \sin\theta\mathbf{e}_\theta)$ is the rotation vector, its absolute value $\Omega = |\boldsymbol{\Omega}|$ is the rate of rotation about the polar axis, p is the pressure deviation from $p_0 = \rho_0 g(R-r) + \frac{\rho_0\Omega^2 r^2\sin^2\theta}{2}$, $\mathbf{r} = r\mathbf{e}_r + \theta\mathbf{e}_\theta + \varphi\mathbf{e}_\varphi$, ν is the kinematic viscosity of the fluid, κ is the coefficient of thermal diffusivity of the fluid, g is the acceleration due to gravity, ∇ is the gradient operator in spherical coordinates. The effects of the centrifugal buoyancy is introduced into the equations via the term $\boldsymbol{\Omega}\times(\boldsymbol{\Omega}\times\mathbf{r})$, and the Coriolis effect via the term $2\boldsymbol{\Omega}\times\mathbf{u}$.

The equations (2.2.2)–(2.2.4) are written in spherical polar coordinates in a rotating frame of reference. The spatial domain is defined by $r_a < r < r_b$, $0 \le \varphi < 2\pi$, and $0 < \theta < \pi$, where r_a is the radius of the inner sphere, r_b is the radius of the outer sphere, and $\theta = 0$ and $\theta = \pi$ correspond to the north and south poles respectively, while $\theta = \frac{\pi}{2}$ corresponds to the equator. To satisfy our assumptions that the flow preserves symmetries, i.e. rotational symmetry: (for which flows that are invariant under rotation about the polar axis, also called axisymmetric flows) and reflectional symmetry: (flows that are invariant under reflection across the equator defined by $\theta = \frac{\pi}{2}$), the variables satisfy the following relations:

$$\begin{aligned} u = u(r,\theta,t) = u(r,\pi-\theta,t), \qquad & v = v(r,\theta,t) = v(r,\pi-\theta,t),\\ w = w(r,\theta,t) = w(r,\pi-\theta,t), \qquad & T = T(r,\theta,t) = T(r,\pi-\theta,t), \qquad (2.2.5)\end{aligned}$$

where the variables u, v, w, T are independent of φ. The spatial range of θ as a result of reflectional symmetry is now $0 \leq \theta \leq \frac{\pi}{2}$, and the spatial domain is now redefined as: $r_a \leq r \leq r_b$, $0 \leq \theta \leq \frac{\pi}{2}$. The symmetries significantly reduce the size of the computational domain and therefore simplify the problem analysis.

We consider two sets of boundary conditions on the fluid velocity on the inner boundary of the spherical shell. That is, the no-slip and the stress-free boundary conditions. By no-slip we mean, the fluid and the solid boundary will have the same velocity; while in the case of stress-free, the boundary does not impose a stress on the fluid. The full set of boundary conditions for the no-slip case are:

$$\begin{aligned}
\mathbf{u} &= 0, && \text{on} \quad r = r_a, \\
\frac{\partial T}{\partial t} = D_R \left(\frac{\partial^2}{\partial r^2} + \frac{2}{r}\frac{\partial}{\partial r} \right) T + D_H \left(\frac{1}{r^2}\frac{\partial^2}{\partial \theta^2} + \frac{\cos\theta}{r^2 \sin\theta}\frac{\partial}{\partial \theta} \right) T & \\
-s_w \left(I(\theta) - QaS(\theta) \right) & && \text{on} \quad r = r_a, \\
\frac{\partial u}{\partial r} - \frac{u}{r} = 0, \quad \frac{\partial v}{\partial r} - \frac{v}{r} = 0, \quad w = 0 & && \text{on} \quad r = r_b, \\
\frac{\partial T}{\partial r} = 0 & && \text{on} \quad r = r_b, \quad (2.2.6)
\end{aligned}$$

and for the stress-free case

$$\begin{aligned}
\frac{\partial u}{\partial r} - \frac{u}{r} = 0, \quad \frac{\partial v}{\partial r} - \frac{v}{r} = 0, \quad w = 0 & && \text{on} \quad r = r_a, \\
\frac{\partial T}{\partial t} = D_R \left(\frac{\partial^2}{\partial r^2} + \frac{2}{r}\frac{\partial}{\partial r} \right) T + D_H \left(\frac{1}{r^2}\frac{\partial^2}{\partial \theta^2} + \frac{\cos\theta}{r^2 \sin\theta}\frac{\partial}{\partial \theta} \right) T & \\
-s_w \left(I(\theta) - QaS(\theta) \right) & && \text{on} \quad r = r_a, \\
\frac{\partial u}{\partial r} - \frac{u}{r} = 0, \quad \frac{\partial v}{\partial r} - \frac{v}{r} = 0, \quad w = 0 & && \text{on} \quad r = r_b, \\
\frac{\partial T}{\partial r} = 0, & && \text{on} \quad r = r_b, \quad (2.2.7)
\end{aligned}$$

where $I(\theta) = A + BT(\theta)$, $S(\theta) = \frac{1}{2}(1 - \cos 2\theta)$, D_R is the diffusion coefficient in the vertical direction, D_H is the diffusion coefficient in the horizontal direction, and s_w is a parameter that is used to switch between the physical scale and laboratory scale of the solar radiation effects. The radiative forcing equation is the boundary equation for the inner surface of the spherical shell.

We replace the Laplacian operators in the equations (2.2.2)–(2.2.4) and boundary conditions (2.2.6)–(2.2.7) with their equivalents in spherical polar coordinates as out-

lined in [3], ignoring the derivatives with respect to the azimuthal components. Thus we have,

$$\begin{aligned}
\nabla^2\mathbf{u} &= \nabla^2\mathbf{u}_r + \nabla^2\mathbf{u}_\theta + \nabla^2\mathbf{u}_\varphi,\\
\nabla^2\mathbf{u}_r &= -\frac{2}{r^2} + \frac{2}{r}\frac{\partial w}{\partial r} + \frac{\partial^2 w}{\partial r^2} + \frac{\cos\theta}{r^2\sin\theta}\frac{\partial w}{\partial\theta} + \frac{1}{r^2}\frac{\partial^2 w}{\partial\theta^2} - \frac{2}{r^2}\frac{\partial v}{\partial\theta} - \frac{2\cos\theta}{r^2\sin\theta}v,\\
\nabla^2\mathbf{u}_\theta &= \frac{2}{r}\frac{\partial v}{\partial r} + \frac{\partial^2 v}{\partial r^2} + \frac{\cos\theta}{r^2\sin\theta}\frac{\partial v}{\partial\theta} + \frac{1}{r^2}\frac{\partial^2 v}{\partial\theta^2} - \frac{1}{r^2\sin^2\theta}v + \frac{2}{r^2}\frac{\partial w}{\partial\theta},\\
\nabla^2\mathbf{u}_\varphi &= \frac{2}{r}\frac{\partial u}{\partial r} + \frac{\partial^2 u}{\partial r^2} + \frac{\cos\theta}{r^2\sin\theta}\frac{\partial u}{\partial\theta} + \frac{1}{r^2}\frac{\partial^2 u}{\partial\theta^2} - \frac{1}{r^2\sin^2\theta}u,
\end{aligned} \tag{2.2.8}$$

$$\boldsymbol{\Omega}\times\mathbf{u} = (-2\Omega\sin\theta u)_r + (2\Omega\cos\theta u)_\theta + 2\Omega(\cos\theta v + \sin\theta w)_\varphi, \tag{2.2.9}$$

$$\boldsymbol{\Omega}\times(\boldsymbol{\Omega}\times\mathbf{r}) = -(\Omega^2 r\sin^2\theta)_r + (\Omega^2 r\sin\theta\cos\theta)_\theta, \tag{2.2.10}$$

$$\begin{aligned}
(\mathbf{u}\cdot\nabla)\mathbf{u} &= \left(w\frac{\partial}{\partial r} + \frac{v}{r}\frac{\partial}{\theta} + \frac{u}{r\sin\theta}\frac{\partial}{\partial\varphi}\right)w\mathbf{e}_r + \left(w\frac{\partial}{\partial r} + \frac{v}{r}\frac{\partial}{\theta} + \frac{u}{r\sin\theta}\frac{\partial}{\partial\varphi}\right)v\mathbf{e}_\theta\\
&\quad + \left(w\frac{\partial}{\partial r} + \frac{v}{r}\frac{\partial}{\theta} + \frac{u}{r\sin\theta}\frac{\partial}{\partial\varphi}\right)u\mathbf{e}_\varphi,
\end{aligned} \tag{2.2.11}$$

where $(\,\cdot\,)_r$, $(\,\cdot\,)_\theta$ and $(\,\cdot\,)_\varphi$ denotes r, θ and φ components respectively. The derivatives of the unit vectors in the convective term are non-vanishing, and we have replaced them as follows:

$$\begin{aligned}
\frac{\partial\mathbf{e}_r}{\partial r} &= 0,\ \frac{\partial\mathbf{e}_\theta}{\partial r} = 0,\ \frac{\partial\mathbf{e}_\varphi}{\partial r} = 0,\\
\frac{\partial\mathbf{e}_r}{\partial\theta} &= \mathbf{e}_\theta,\ \frac{\partial\mathbf{e}_\theta}{\partial\theta} = -\mathbf{e}_r,\ \frac{\partial\mathbf{e}_\varphi}{\partial\theta} = 0,\\
\frac{\partial\mathbf{e}_r}{\partial\varphi} &= \mathbf{e}_\varphi\sin\theta,\ \frac{\partial\mathbf{e}_\theta}{\partial\varphi} = \mathbf{e}_\varphi\cos\theta,\\
\frac{\partial\mathbf{e}_\varphi}{\partial\varphi} &= -(\mathbf{e}_r\sin\theta + \mathbf{e}_\theta\cos\theta).
\end{aligned} \tag{2.2.12}$$

If we scale the radial coordinate as

$$r \to Rr',$$

where $R = r_b - r_a$ is the gap width, re-write the temperature as

$$T \to T' + T_r - q\cos 2\theta, \tag{2.2.13}$$

where q is the differential heating parameter that will be related to the solar constant Q below, substitute these into equations (2.2.2) – (2.2.4), and drop the primes, we

obtain the following axisymmetric equations:

$$\begin{aligned}\frac{\partial u}{\partial t} &= \nu_s\nabla_0^2 u - \nu_s\frac{1}{r^2\sin^2\theta}u - 2\Omega\left(\sin\theta w + \cos\theta v\right)\\ &\quad -\frac{1}{R}\left[\left(\mathbf{u}\cdot\nabla_0\right)u + \frac{\cos\theta}{r\sin\theta}uv + \frac{uw}{r}\right], \qquad (2.2.14)\\ \frac{\partial v}{\partial t} &= \nu_s\nabla_0^2 v - \nu_s\left(\frac{1}{r^2\sin^2\theta}v - \frac{2}{r^2}\frac{\partial w}{\partial\theta}\right) + 2\Omega\cos\theta u - \frac{1}{\rho_0 Rr}\frac{\partial p}{\partial\theta}\\ &\quad -\left(\alpha\Omega^2 Rr\sin\theta\cos\theta\right)\left(T - q\cos 2\theta\right) - \frac{1}{R}\left[\left(\mathbf{u}\cdot\nabla_0\right)v - \frac{\cos\theta}{r\sin\theta}u^2 + \frac{vw}{r}\right], \qquad (2.2.15)\\ \frac{\partial w}{\partial t} &= \nu_s\nabla_0^2 w - \nu_s\left(\frac{2}{r^2}\frac{\cos\theta}{\sin\theta}v + \frac{2}{r^2}\frac{\partial v}{\partial\theta} + \frac{2}{r^2}w\right) + 2\Omega\sin\theta u - \frac{1}{\rho_0 Rr}\frac{\partial p}{\partial r}\\ &\quad -\alpha\left(\Omega^2 Rr\sin^2\theta + g\right)\left(T - q\cos 2\theta\right) - \frac{1}{R}\left[\left(\mathbf{u}\cdot\nabla_0\right)w - \frac{1}{r}\left(u^2+v^2\right)\right], \qquad (2.2.16)\\ \frac{\partial T}{\partial t} &= \kappa_s\nabla_0^2 T + \frac{4q\kappa_s}{r^2}(\cos 2\theta + \cos^2\theta + \frac{2q}{Rr}\sin 2\theta v) - \frac{1}{R}\left(\mathbf{u}\cdot\nabla_0\right)T, \qquad (2.2.17)\\ \nabla_0\cdot\mathbf{u} &= \frac{\partial w}{\partial r} + \frac{2}{r}w + \frac{1}{r}\frac{\partial v}{\partial\theta} + \frac{\cos\theta}{r\sin\theta}v = 0, \qquad (2.2.18)\end{aligned}$$

where $\nu_s = \nu/R^2$, $\kappa_s = \kappa/R^2$,

$$\nabla_0^2 = \frac{\partial^2}{\partial r^2} + \frac{2}{r}\frac{\partial}{\partial r} + \frac{1}{r^2}\frac{\partial^2}{\partial\theta^2} + \frac{\cos\theta}{r^2\sin\theta}\frac{\partial}{\partial\theta}, \qquad (2.2.19)$$

$$\nabla_0 = \mathbf{e}_r\frac{\partial}{\partial r} + \mathbf{e}_\theta\frac{1}{r}\frac{\partial}{\partial\theta}, \qquad (2.2.20)$$

and

$$\left(\mathbf{u}\cdot\nabla_0\right)f = w\frac{\partial f}{\partial r} + \frac{v}{r}\frac{\partial f}{\partial\theta}, \qquad (2.2.21)$$

for any scalar function $f = f(r,\theta,t)$.

The symmetry assumptions effectively introduce new boundary conditions at the equator and the pole. In order to satisfy the symmetries, no flow of fluid and heat across the equator and the pole is allowed. Also, the effects of boundary layers on the fluid flow are ignored with stress-free boundary conditions imposed on the fluid velocities at the inner and outer boundaries of the shell. In addition, the conditions $u = 0, v = 0$ at the pole are necessary to ensure that no discontinuity occurs in the

fluid velocity at the pole. Thus, we have the additional boundary conditions:

$$\begin{aligned} u, v = 0, \qquad \frac{\partial w}{\partial \theta} = 0, \qquad \frac{\partial T}{\partial \theta} = 0 \qquad &\text{on} \quad \theta = 0, \\ v = 0, \qquad \frac{\partial u}{\partial \theta} = \frac{\partial w}{\partial \theta} = 0, \qquad \frac{\partial T}{\partial \theta} = 0 \qquad &\text{on} \quad \theta = \frac{\pi}{2}. \end{aligned} \tag{2.2.22}$$

2.2.1 The Steady Axisymmetric Solution

We begin the investigation of our model with the computation of the steady axisymmetric solutions that are invariant with respect to reflection across the equator; that is, we seek solutions of (2.2.14) – (2.2.18) that are independent of time and that satisfy the boundary conditions (2.2.6) and (2.2.22) for the no-slip case, and (2.2.7) and (2.2.22) for the stress-free case.

The method of stream functions is used to solve the steady equations. If v and w are written in terms of a stream function ξ, defined by

$$v = -\frac{\xi}{r} - \frac{\partial \xi}{\partial r}, \qquad w = \frac{1}{r}\frac{\partial \xi}{\partial \theta} + \frac{1}{r}\frac{\cos\theta}{\sin\theta}\xi, \tag{2.2.23}$$

then the incompressibility condition (2.2.18) is automatically satisfied. After using (2.2.23) to replace v and w in the equations, the pressure terms can be eliminated. Subsequently, the steady solution can be found from the resulting three equations in the three unknown functions u, ξ and T. The boundary conditions for u and T are given by equations (2.2.6)–(2.2.7) and (2.2.22) as before, while the conditions on v and w will be satisfied if ξ satisfies the boundary conditions: for no-slip,

$$\begin{aligned} \xi = 0, \qquad \frac{\partial \xi}{\partial \theta} = 0, \qquad \frac{\partial^3 \xi}{\partial \theta^3} = 0 \qquad &\text{on} \quad \theta = 0, \\ \xi = 0, \qquad \frac{\partial^2 \xi}{\partial \theta^2} = 0 \qquad &\text{on} \quad \theta = \frac{\pi}{2}, \\ \xi = 0, \qquad \frac{\partial^2 \xi}{\partial r^2} = 0 \qquad &\text{on} \quad r = \frac{r_b}{R}, \\ \xi = 0, \qquad \frac{\partial \xi}{\partial r} = 0 \qquad &\text{on} \quad r = \frac{r_a}{R}, \end{aligned} \tag{2.2.24}$$

and for stress-free,

$$\begin{aligned}
&\xi = 0, \qquad \frac{\partial \xi}{\partial \theta} = 0, \qquad \frac{\partial^3 \xi}{\partial \theta^3} = 0 \qquad \text{on} \quad \theta = 0, \\
&\xi = 0, \qquad \frac{\partial^2 \xi}{\partial \theta^2} = 0 \qquad \text{on} \quad \theta = \frac{\pi}{2}, \\
&\xi = 0, \qquad \frac{\partial^2 \xi}{\partial r^2} = 0 \qquad \text{on} \quad r = \frac{r_a}{R}, \ \frac{r_b}{R}.
\end{aligned} \tag{2.2.25}$$

2.3 Analysis of the Radiative Boundary Equation

A critical look into the radiative equation in its steady state is necessary in order to adapt it to the model studied here and to choose the appropriate values for the equation parameters. In view of this, we consider the radiative boundary equation

$$\begin{aligned}
D_R \left(\frac{\partial^2}{\partial r^2} + \frac{2}{r} \frac{\partial}{\partial r} \right) T + D_H \left(\frac{1}{r^2} \frac{\partial^2}{\partial \theta^2} + \frac{\cos\theta}{r^2 \sin\theta} \frac{\partial}{\partial \theta} \right) T \\
- s_w \left(I(\theta) - QaS(\theta) \right) = 0,
\end{aligned} \tag{2.3.1}$$

for both stress-free and no-slip cases.

By substituting $T \to T' + T_r - q\cos 2\theta$ and $r \to Rr'$ into equation (2.3.1) and also replacing S and a as described in Section 2.1, we have

$$\begin{aligned}
D_{R0} \left(\frac{\partial^2}{\partial r^2} + \frac{2}{r} \frac{\partial}{\partial r} \right) T + D_{H0} \left(\frac{1}{r^2} \frac{\partial^2}{\partial \theta^2} + \frac{\cos\theta}{r^2 \sin\theta} \frac{\partial}{\partial \theta} \right) T + \frac{4qD_{H0}}{r^2} \left(\cos 2\theta + \cos^2\theta \right) \\
- s_w \left(A + B(T + T_r) - qB\cos 2\theta - \frac{0.38Q}{2} + \frac{0.38Q\cos 2\theta}{2} \right) \\
- s_w \left(\frac{0.3Qc(1 - \cos 2\theta)H_m}{2} \right) = 0,
\end{aligned} \tag{2.3.2}$$

where $D_{R0} = \frac{D_R}{R^2}$, $D_{H0} = \frac{D_H}{R^2}$ and c is a parameter to switch off and on the contributions of the Hill function; it takes value $c = 1$ if the Hill function is on, and $c = 0$ if the Hill function is off. In equation (2.3.2), we want a linear relationship between the differential heating q and the solar constant Q, and we set

$$qB\cos 2\theta = \frac{0.38Q\cos 2\theta}{2},$$

and therefore

$$qB = \frac{0.38Q}{2}, \tag{2.3.3}$$

$$Q = \frac{2Bq}{0.38}. \tag{2.3.4}$$

Equation (2.3.4) shows a linear relationship between the solar constant Q and the differential heating parameter q, therefore, an increase in q means an increase in Q, and vice versa. With relationship (2.3.4), the actual solar constant $Q = 0.14\text{Wcm}^{-2}$ corresponds to the differential heating $q = 0.018$. We shall not be able to increase the differential heating to $q = 0.018$, because the geometry and parameter values for the model are far from those of the earth. Equation (2.3.2) becomes

$$D_{R0}\left(\frac{\partial^2}{\partial r^2} + \frac{2}{r}\frac{\partial}{\partial r}\right)T + D_{H0}\left(\frac{1}{r^2}\frac{\partial^2}{\partial\theta^2} + \frac{\cos\theta}{r^2\sin\theta}\frac{\partial}{\partial\theta}\right)T + \frac{4qD_{H0}}{r^2}\left(\cos 2\theta + \cos^2\theta\right) - s_w\left(A + B(T + T_r) - qB - \frac{0.3qBc(1-\cos 2\theta)H_m}{0.38}\right) = 0, \tag{2.3.5}$$

where

$$H_m = \frac{(T + T_r - q\cos 2\theta)^m}{T_0^m + (T + T_r - q\cos 2\theta)^m}. \tag{2.3.6}$$

We need to choose values of the parameter in equation (2.3.5), and a critical value for the ice boundary temperature T_0, that will give a desired radiative forcing. If the quantity of the differential heating q is still very small, there is an outgoing radiation of $-A$. In order to avoid this, the temperature T is scaled as $T \to \frac{T'}{B} - \frac{A}{B}$. This scaling eliminates A from the boundary equation.

Thus, after dropping primes, we have the equation for the temperature deviation T at the inner boundary:

$$D_R\left(\frac{\partial^2}{\partial r^2} + \frac{2}{r}\frac{\partial}{\partial r}\right)T + D_H\left(\frac{1}{r^2}\frac{\partial^2}{\partial\theta^2} + \frac{\cos\theta}{r^2\sin\theta}\frac{\partial}{\partial\theta}\right)T + \frac{4qD_H}{r^2}\left(\cos 2\theta + \cos^2\theta\right) - s_w\left(B(\frac{T}{B} + T_r) - qB - \frac{0.3qBc(1-\cos 2\theta)H_m}{0.38}\right) = 0, \tag{2.3.7}$$

where $D_R = \frac{D_{R0}}{B}$, $D_H = \frac{D_{H0}}{B}$, and the Hill function remains as in equation (2.3.6), i.e. the T and T_0 in the Hill function are not scaled as this does not alter the dynamics of

the system.

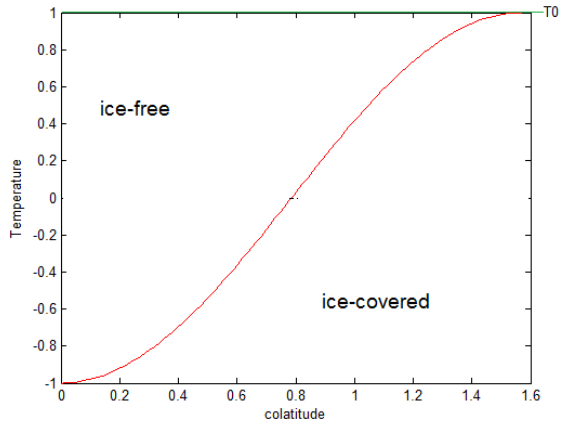

Figure 2.2: An illustrative plot of the ice-boundary temperature against colatitudinal temperature distribution, where T is the temperature before the scaling (see equation (2.3)).

It is important to discuss the role of the ice boundary T_0 in the boundary equation. Figure 2.2 shows the critical ice boundary temperature T_0 against the temperature distribution. For this project, we assume T_0 to be any reasonable value between 0 and 1 for the temperature of the ice boundary, that is, a situation where there is an ice sheet at the polar region and the equatorial region is ice-free. This is the situation in the present-day climate. If the value of T_0 is taken to be larger than its current value, it implies that ice would form and its boundary would shift towards the equator. If the value of T_0 is taken smaller, it means the ice sheet's boundary is shifting towards the pole. For sufficiently small T_0, no ice forms, and the climate is said to be undergoing an ice-free regime, and for those values of T_0 that are sufficiently large, ice will extend towards the equator, the climate is said to be undergoing an ice-age regime. In Chapter 4 we show the results for different values of T_0 and how they affect the mean temperature of the system.

Chapter 3

The Pseudo Arc-length Continuation Method

3.1 Numerical Discretization

As the terms in the model appear in various forms of nonlinearity, it is necessary to replace each of the terms with their equivalent numerical derivatives. As such we will be able to approximate the solution of the resulting system of nonlinear equations at certain grid points within the computational domain. The use of numerical derivatives is necessary because analytical solutions of the system of partial differential equations (i.e. the Navier Stokes equations) are not possible to find. There are several forms of numerical derivatives, e.g. forward finite differences, backward finite differences and centered finite differences. For this work, second order centered finite difference formulae are used. This choice is based on the second order property which enables a relatively quick convergence, i.e. the error becomes small for a reasonable step size (or mesh size). In this chapter, we discuss the numerical methods that are implemented. In particular, we discuss centered finite differencing, the discretization of the partial derivatives, Newton's method for computing solutions of nonlinear systems of equations and the pseudo arc-length continuation technique for computing solutions as a parameter of the system is varied.

3.2 Centered Finite Differencing

Consider a function $f(r,\theta)$ defined on $r \in \left[\frac{r_a}{R}, \frac{r_b}{R}\right]$, $\theta \in \left[0, \frac{\pi}{2}\right]$ which is partitioned into a uniform grid, i.e. the grid points are equally spaced at a distance h in both r and θ variables. Suppose $f(r,\theta)$ is evaluated at two points in the neighborhood of (r,θ), i.e. $f(r-h,\theta)$ and $f(r+h,\theta)$.

Applying Taylor's Expansion Theorem to each of these perturbed functions, we have:

$$f(r-h,\theta) = f(r,\theta) - \frac{\partial f(r,\theta)}{\partial r}h + \frac{\partial^2 f(r,\theta)}{\partial r^2}\frac{h^2}{2!} - \frac{\partial^3 f(r,\theta)}{\partial r^3}\frac{h^3}{3!} + ..., \tag{3.2.1}$$

$$f(r+h,\theta) = f(r,\theta) + \frac{\partial f(r,\theta)}{\partial r}h + \frac{\partial^2 f(r,\theta)}{\partial r^2}\frac{h^2}{2!} + \frac{\partial^3 f(r,\theta)}{\partial r^3}\frac{h^3}{3!} + ... \tag{3.2.2}$$

Subtracting (3.2.1) from (3.2.2) and dividing by $2h$, we can obtain:

$$\frac{\partial f(r,\theta)}{\partial r} = \frac{f(r+h,\theta) - f(r-h,\theta)}{2h} + O(h^2). \tag{3.2.3}$$

Adding equations (3.2.1) and (3.2.2) and dividing by h^2, we can obtain:

$$\frac{\partial^2 f(r,\theta)}{\partial r^2} = \frac{f(r-h,\theta) - 2f(r,\theta) + f(r+h,\theta)}{h^2} + O(h^2). \tag{3.2.4}$$

where $O(h^2) = Ch^2$, and C is proportional to the leading derivative in the truncated part of the series, evaluated at some point $r \in (\frac{r_a}{R}, \frac{r_b}{R})$. Upon truncation of the terms of order $O(h^2)$, these so-called centered finite difference formulae can be used to approximate the indicated derivatives. Higher order and mixed derivatives can be derived by the method of undetermined multipliers as shown in [19]. The derivation is also similar for derivatives with respect to more than one variable. The higher order derivatives in one variable are:

$$\frac{\partial^3 f(r,\theta)}{\partial r^3} = \frac{f(r+2h,\theta) - 2f(r+h,\theta) + 2f(r-h,\theta) - f(r-2h,\theta)}{2h^3} + O(h^2),$$

$$\frac{\partial^4 f(r,\theta)}{\partial r^4} = \frac{f(r+2h,\theta) - 2f(r+h,\theta) + 6f(r,\theta) - 4f(r-h,\theta)}{2h^3} \\ \frac{-f(r-2h,\theta)}{2h^3} + O(h^2). \tag{3.2.5}$$

3.2.1 Error Analysis

Neglecting the $O(h^2)$ terms in the expressions for the derivatives (3.2.3)–(3.2.5) leads to error. This error, called *truncation error*, is a function of the grid spacing (mesh size) h. Round-off error is a result of the limitation in computing machines. It depends on the floating point number representation of the machine on which the computation is carried out (single or double precision). Due to round-off error, significant digits

are lost in the evaluation of the function values of the centered differences. The total error in any numerical computation is the aggregate of truncation and round-off errors, which are independent of each other.

Consider, for example, the truncation error in the formula for the first derivative.

$$\frac{\partial f(r,\theta)}{\partial r} = \frac{f(r+h,\theta) - f(r-h,\theta)}{2h} + \frac{\partial^3 f(r,\theta)}{\partial r^3}\frac{h^2}{2(3!)} + ... \tag{3.2.6}$$

The local truncation error in (3.2.6) can be written as:

$$E_T(h) = Ch^2 \equiv O(h^2), \tag{3.2.7}$$

where $C = \frac{1}{2(3!)}\frac{\partial^3 f(r,\theta)}{\partial r^3}|_{\theta,r=\xi}$ is a constant evaluated in the interval $r \in \left[\frac{r_a}{R}, \frac{r_b}{R}\right]$. Also, suppose that each function evaluation in (3.2.6) has a rounding error of ε, then the round-off error in the first derivative can be written as:

$$E_R(h) = \frac{\varepsilon + \varepsilon}{2h} = \frac{\varepsilon}{h}. \tag{3.2.8}$$

Therefore, the total error can be written as follows:

$$E_{total} = E_T(h) + E_R(h) = Ch^2 + \frac{\varepsilon}{h}. \tag{3.2.9}$$

It is obvious from equation (3.2.9) that there is a dilemma as regards to the choice of the size of h that minimizes the total error. As $h \to 0$, the truncation error decreases and the truncated Taylor series gives a better approximation to the derivatives, but at the same time, the round-off error increases causing the error in the numerical solution to grow. To overcome this, the choice of h must be a compromise chosen to balance these two sources of error. The critical value of h at which E_{total} is minimum is the point

$$\frac{dE_{total}}{dh} = 2Ch - \frac{\varepsilon}{h^2} = 0, \tag{3.2.10}$$

and

$$h_{optimum} = \left(\frac{\varepsilon}{2C}\right)^{\frac{1}{3}}, \tag{3.2.11}$$

such that

$$\frac{d^2 E_{total}(h_{optimum})}{dh^2} = 6C, \tag{3.2.12}$$

where $h_{optimum}$ is the optimal mesh size $h = \frac{1}{N+1}$ and $C > 0$.

3.3 Discretization of PDE

For all computations in this thesis, the domain of computation is equally partitioned for both the θ and r coordinates, with step size h. We have three unknown variables ξ, u, and T, which are concatenated into vector form as $X = [\xi, u, T]^T$. For both no-slip and stress-free cases, each variable ξ, u, T, is discretized at $N \times N$ interior grid points. Also, for both choices of boundary conditions on the inner boundary, the values of ξ are specified at the points on the boundary, but values of the temperature deviation T at the points on the boundary are not specified, hence, there are an extra $4N + 4$ unknown variables. In the case of the variable u, for the stress-free case, its values are specified at $\theta = 0$, but unknown for all other boundary points. This adds an additional $3N + 2$ unknown variables. Similarly, for the no-slip case, the values of u, are specified at both $\theta = 0$ and $r = \frac{r_a}{R}$, but unknown for all other boundary points. This adds an additional $2N + 1$ unknown variables. The total number of unknown variables is $\Sigma = 3N^2 + 7N + 6$ (if the boundary condition on velocity at $r = \frac{r_a}{R}$ is stress-free) or $\Sigma = 3N^2 + 6N + 5$ (if boundary condition on velocity at $r = \frac{r_a}{R}$ is no-slip). Since the equation is evaluated at each grid point, Σ nonlinear algebraic equations in Σ unknowns are solved using Newton's Method and Keller's Continuation, as described in Section 3.4 and Section 3.5, respectively.

Define

$$f(r_i, \theta_j) = f_{i,j}$$

for some arbitrary function f where $r_i = \frac{r_a}{R} + ih$ and $\theta_j = \frac{\pi ik}{2}$, $0 \leq i, j \leq N + 1$ and let equations (2.2.14)–(2.2.18), which can be written as

$$F(x(r, \theta)) = 0, \tag{3.3.1}$$

be the nonlinear equation that is solved for the axisymmetric solution $x = [\xi, u, T]^T$. Assuming $k = h$, the different orders of the partial derivatives of ξ, u, T in (3.3.1) can be replaced with their corresponding difference approximations:

$$\begin{aligned}
\frac{\partial f}{\partial r} &= \frac{f_{i+1,j} - f_{i-1,j}}{2h}, \\
\frac{\partial^2 f}{\partial r^2} &= \frac{f_{i+1,j} - 2f_{i,j} + f_{i-1,j}}{h^2}, \\
\frac{\partial^3 f}{\partial r^3} &= \frac{f_{i+2,j} - 2f_{i+1,j} + 2f_{i-1,j} - f_{i-2,j}}{2h^3}, \\
\frac{\partial^4 f}{\partial r^4} &= \frac{f_{i+2,j} - 4f_{i+1,j} + 6f_{i,j} - 4f_{i-1,j} + f_{i-2,j}}{h^4}, \\
\frac{\partial f}{\partial \theta} &= \frac{f_{i,j+1} - f_{i,j-1}}{2h}, \\
\frac{\partial^2 f}{\partial \theta^2} &= \frac{f_{i,j+1} - 2f_{i,j} + f_{i,j-1}}{h^2}, \\
\frac{\partial^3 f}{\partial \theta^3} &= \frac{f_{i,j+2} - 2f_{i,j+1} + 2f_{i,j-1} - f_{i,j-2}}{2h^3}, \\
\frac{\partial^4 f}{\partial \theta^4} &= \frac{f_{i,j+2} - 4f_{i,j+1} + 6f_{i,j} - 4f_{i,j-1} + f_{i,j-2}}{h^4}, \\
\frac{\partial^2 f}{\partial r \partial \theta} &= \frac{f_{i+1,j+1} - f_{i-1,j+1} - f_{i+1,j-1} - f_{i-1,j-1}}{4h^2}, \\
\frac{\partial^3 f}{\partial r^2 \partial \theta} &= \frac{f_{i+1,j+1} - 2f_{i+1,j} + f_{i+1,j-1} - f_{i-1,j+1} + 2f_{i-1,j} - f_{i-1,j-1}}{2h^3}, \\
\frac{\partial^3 f}{\partial \theta^2 \partial r} &= \frac{f_{i+1,j+1} - 2f_{i,j+1} + f_{i-1,j+1} - f_{i+1,j-1} + 2f_{i,j-1} - f_{i-1,j-1}}{2h^3},
\end{aligned} \tag{3.3.2}$$

$$\begin{aligned}
\frac{\partial^4 f}{\partial r^2 \partial \theta^2} = \frac{f_{i+1,j+1} - 2f_{i,j+1} + f_{i-1,j+1} - 2f_{i+1,j} + 4f_{i,j}}{h^4} \\
\frac{-2f_{i-1,j} + f_{i+1,j-1} - 2f_{i,j-1} + f_{i-1,j-1}}{h^4}.
\end{aligned}$$

Thus, we obtain a system of nonlinear algebraic equations:

$$\mathbf{F}(\mathbf{x}) = \mathbf{0}, \tag{3.3.3}$$

where $\mathbf{F} \in \mathbb{R}^{\Sigma}$ and $\mathbf{x} \in \mathbb{R}^{\Sigma}$ is a vector with components being the unknowns $x_{i,j} = [\xi_{i,j}, u_{i,j}, T_{i,j}]^T$, $0 \le i, j \le N+1$. We solve for the $x_{i,j}$ for all $0 \le i, j \le N+1$.

3.4 Newton's Method

The idea of Newton's method is to linearize the system of nonlinear algebraic equations and solve repeatedly until the difference between the approximation at the current step and that of the previous step meet a certain criteria. The choice of stopping criteria depends on the degree of accuracy needed for the solution, the nature of the problem, or some other limiting physical factors arising from the computational hardware.

To discuss the numerical method, it is convenient to consider a general system of nonlinear equations expressed in vector form as:

$$\mathbf{F}(\mathbf{x}) = \mathbf{0}, \tag{3.4.1}$$

where $\mathbf{x}$ is the solution of (3.4.1), $\mathbf{x} = (x_1, x_2, x_3, ...x_n)$ and $\mathbf{F} = (f_1, f_2, f_3, ...f_n)^T$. Let (3.4.1) be perturbed as $\mathbf{F}(\mathbf{x} + \mathbf{h})$, where $\mathbf{x}$ is some approximate or guess of the solution, and approximate it using the first two terms of its Taylor series expansion:

$$\mathbf{0} = \mathbf{F}(\mathbf{x} + \mathbf{h}) \approx \mathbf{F}(\mathbf{x}) + \mathbf{F}'(\mathbf{x})\mathbf{h}. \tag{3.4.2}$$

The perturbation (also called the correction vector) of $\mathbf{x}$ is $\mathbf{h} = (h_1, h_2, h_3, ...h_n)$, and $\mathbf{F}'(\mathbf{x})$ is the matrix of partial derivatives of $\mathbf{F}$ with respect to $\mathbf{x}$, called the *Jacobian matrix*. Solving the system of linear equations (3.4.2) for $\mathbf{h}$, we have:

$$\mathbf{h} = -\mathbf{F}'(\mathbf{x})^{-1}\mathbf{F}(\mathbf{x}). \tag{3.4.3}$$

To be able to find $\mathbf{h}$ it is required that $\mathbf{F}'(\mathbf{x})$ in (3.4.3) be nonsingular. For a large system of equations, it is computationally expensive to compute the inverse. Thus instead, the system is written as a system of n linear equations in n unknown variables:

$$\mathbf{F}'(\mathbf{x}^{(k)})\mathbf{h}^{(k)} = -\mathbf{F}(\mathbf{x}^{(k)}), \tag{3.4.4}$$

where the updated approximation is given by

$$\mathbf{x}^{(k+1)} = \mathbf{x}^{(k)} + \mathbf{h}^{(k)}, \tag{3.4.5}$$

where k is the iteration count. The $\mathbf{x}^{(0)}$ is the initial guess for Newton's iteration. This method is guaranteed to converge provided the initial guess is sufficiently close to the

solution, and $\mathbf{F}'(\mathbf{x}^{(k)})$ is nonsingular. The system (3.4.4) can be solved using Gaussian elimination or some other suitable method.

3.5 The Pseudo Arc-length Continuation Method

Consider the nonlinear system of equations in (3.4.1) whose solution is to be found for different values of a bifurcation parameter q (e.g. the differential heating). The equation can be re-written as:

$$F(\mathbf{x}, q) = 0, \tag{3.5.1}$$

where $\mathbf{x} \in \mathbb{R}^n$, $q \in \mathbb{R}$ and $F(\mathbf{x}, q) \in \mathbb{R}^n$. To successfully follow the solution of $F(\mathbf{x}, q)$ for different values of the bifurcation parameter q, we use the pseudo-arc length continuation method, at the heart of which is the idea of bordered matrices. The method is a technique to find consecutive points of a solution branch to (3.5.1), and is adapted in this work as stated in [6, 1].

Consider the solution $\mathbf{x}$ and the parameter q as functions of s, i.e. $\mathbf{x} = \mathbf{x}(s)$ and $q = q(s)$. Differentiation of (3.5.1) with respect to s leads to:

$$\frac{\partial F}{\partial \mathbf{x}}(\mathbf{x}, q)\frac{d\mathbf{x}}{ds} + \frac{\partial F}{\partial q}(\mathbf{x}, q)\frac{dq}{ds} = 0, \tag{3.5.2}$$

which is a system of n equations in $n+1$ unknowns in $\mathbf{x}$ and q. We choose $t^{(x)T} = \frac{d\mathbf{x}}{ds}$ and $t^q = \frac{dq}{ds}$, such that the tangent at any point on the solution branch is taken as $t = [t^{(x)T}, t^q]^T$. Suppose that a point $(\mathbf{x}_0^T, q_0)$ with tangent vector t_0 and point $(\mathbf{x}_1^T, q_1)$ are known, then the following steps are required:

(1) Find a tangent vector t_1 at $(\mathbf{x}_1^T, q_1)$ by solving the system of equations:

$$\begin{aligned} [F_x, F_q]t_1 &= 0, \\ t_0^T t_1 &= 1. \end{aligned} \tag{3.5.3}$$

The second equation in (3.5.3) is necessary to preserve the direction of the tangents t_0 and t_1, and to make the system $n+1$ equations in $n+1$ unknowns. Then the equations

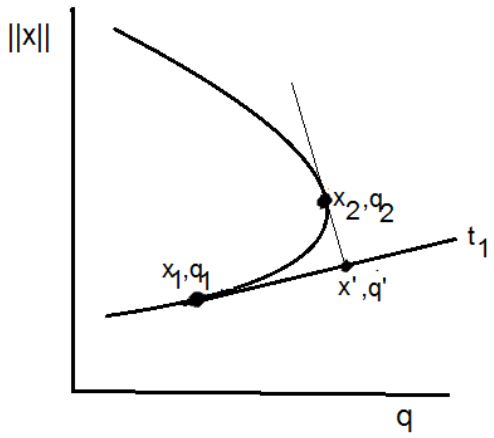

Figure 3.1: A figure illustrating pseudo-arclength continuation.

can be put in matrix form as:

$$\begin{bmatrix} F_x & F_q \\ t_0^{(x)T} & t_0^{(q)} \end{bmatrix} \cdot \begin{bmatrix} t_1^x \\ t_1^q \end{bmatrix} = \begin{bmatrix} 0 \\ 1 \end{bmatrix}. \tag{3.5.4}$$

The matrix in (3.5.4) takes the form of a bordered matrix (as shown below), with borderwidth $m = 1$:

$$\begin{bmatrix} A & B \\ C^T & D \end{bmatrix},$$

where $A \in \mathbb{R}^{n\times n}$, B, $C \in \mathbb{R}^{n\times m}$, and $D \in \mathbb{R}^{m\times m}$. Equation (3.5.4) can be solved using, e.g. the **BEM** (i.e. the Block Elimination Mixed) algorithm as outlined in [6]; the error analysis of **BEM** is detailed in [6, 5].

(2) Predict a new point along the tangent vector t_1 a distance Δs away from (x_1^T, q_1). See Figure 3.1. The predictor is specified as

$$x' = x_1 + \frac{\Delta s}{\|t_1\|} t_1^x, \tag{3.5.5}$$

$$q' = q_1 + \frac{\Delta s}{\|t_1\|} t_1^q. \tag{3.5.6}$$

(3) Correct the predicted point, using Keller's method. We seek the solution in an hyperplane orthogonal to the tangent vector t_1. Thus, we solve the following system

of equations for the next point on the solution branch:

$$F(x,q) = 0,$$
$$t_1^{(x)T}(x - x') + t_1^{(q)T}(q - q') = 0, \tag{3.5.7}$$

with the associated Jacobian :

$$\begin{bmatrix} F_x & F_q \\ t_1^{(x)T} & t_1^{(q)} \end{bmatrix} \tag{3.5.8}$$

Since equation (3.5.7) is nonlinear, it is solved iteratively using Newton's method. The solution of (3.5.7) provides a new point (x_2, q_2) along the solution branch (see Figure 3.1). Steps (1) to (3) can now be repeated using known solutions (x_1, q_1) and (x_2, q_2) to obtain the next point along the branch, and so on. The power of pseudo arc-length continuation arises because the Jacobian (3.5.8) is not singular at limit points along the solution curve, where a limit point is a point at which the curve turns back on itself as depicted in Figure 3.1.

Chapter 4
Results

4.1 Results and Comparisons

In this section, we validate the results of the computation by comparing them with the model studied in [10]. This is made possible by setting appropriate values for some parameters in the radiative forcing equation imposed on the inner boundary of the spherical shell in our model. Table 4.1 shows the values of all parameters used in the computation for both cases of boundary conditions imposed on the lower boundary of the computational domain.

r_a	9	cm
ν	1.01x10^{-2}	cm^2/sec
κ	1.41x10^{-3}	cm^2/sec
α	2.06x10^{-4}	$1/^0C$
ρ_0	0.998	gm cm^3
T_r	0	^{0}C
g	980	cm/sec^2
B	1.45	$Wcm^{-2}/^0$C
D_R	1.21x10^{-2}	cm^2/sec
D_H	1.21x10^{-2}	cm^2/sec

Table 4.1: The table of values for computation. The units are non-SI units because the model is on laboratory scale and similar works used non-SI units [11, 4].

In Table 4.1, the r_a is the radius of the inner sphere, ν is the kinematic viscosity, κ is the coefficient of thermal diffusivity, D_R is the diffusion coefficient in the radial direction, D_H is the diffusion coefficient in the meridional direction, α is the coefficient of thermal expansion, ρ_0 is the density at reference temperature T_r, g is the acceleration due to gravity, and B is the coefficient of linear expansion of outgoing radiation.

The results in [11, 10] are obtained with prescribed temperature, of the form $T = T_r - \Delta T \cos 2\theta$, on the inner boundary of the spherical shell, with the set of equations

(2.2.14)–(2.2.18). In [10], the differential heating parameter is ΔT, and it is the same as the differential heating parameter q in our model. In order to transform our model to the case of the prescribed temperature, the following values are assigned to the radiative forcing equation: $D = 0$, $sw = 1$, $A = 0$, $B = 1$ and $c = 0$, and we have on the inner boundary, $T = -T_r$. We choose $T_r = 0$ so that the temperature deviation from reference temperature on the inner surface is zero for all latitudes, and the differential heating is $2\Delta T$ (or equivalently, $2q$) between the equator and the pole. Obviously, with this set of parameter values, the radial heat exchange between the fluid and the boundary does not affect the temperature at the boundary, the effect of albedo feedback is removed, and the forcing from the boundary increases linearly with the differential heating.

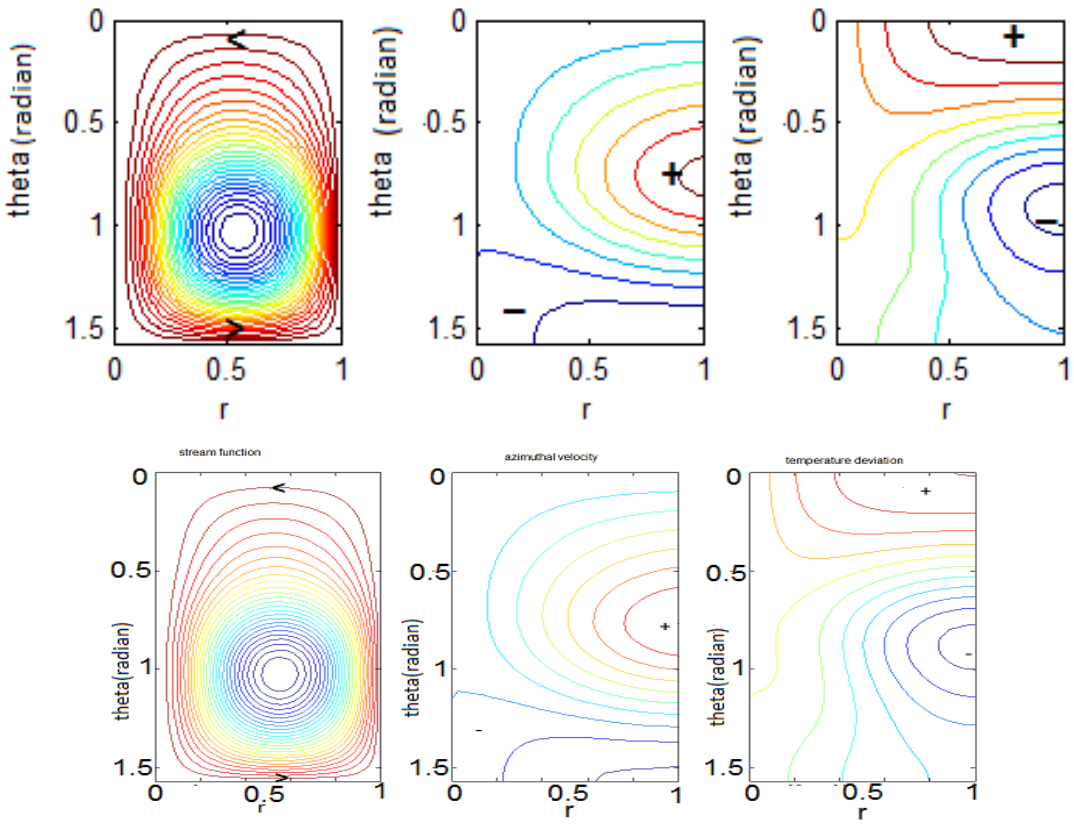

Figure 4.1: (1st row): With prescribed temperature. (2nd row): With radiative forcing. A single-cell circulation pattern observed for heating parameter $q = 0.0017$, gap width $R = 3.4$, rotation rate $\Omega = 0.01$ and with parameters chosen to mimic prescribed temperature on the inner boundary. From left to right, the stream function ξ; the azimuthal velocity u and the temperature deviation T from $-q\cos 2\theta$.

For the solutions (i.e. the contour plots) presented in Figure 4.1 and Figure 4.2, from left to right, we have the stream function $\xi = \xi(r, \theta)$, the azimuthal (zonal) velocity $u = u(r, \theta)$ and the temperature deviation $T = T(r, \theta)$ from the reference profile $T_r - q\cos 2\theta$. The stream function is the combined radial and meridional components of the velocity. Each of the radial and polar components can be recovered by using equation (2.2.23). The fluid flow follows the contour of the stream function ξ. The arrows indicate the directions of motion and the signs '+' and '−' indicate where the functions have their maximum and minimum respectively. For each of the solutions, the result is a cross-section of the flow at an arbitrary value of the zonal (i.e. azimuthal) variable φ. The complete solution for the 3-dimensional problem in equations (2.2.2)–(2.2.4) is obtainable by rotating this cross-sectional solution about the polar axis and reflecting it about the equator. Although the model is studied in a spherical shell, the results are presented in a rectangular domain. This is possible because the symmetric spherical shell and the rectangular region are homeomorphic. By homeomorphic, we mean that the result obtained on the rectangular domain can be mapped to the domain of the spherical shell without any qualitative changes in the solution. For all the results presented in this chapter, we take $N = 40$ and r is a scaled dimensionless variable. The ice boundary temperature is taken as $T_0 = 0^0C$ and this essentially sets the Hill function (i.e. equation (2.1.4)) to unity. Wherever a different value of T_0 is used, its value is given explicitly.

For a single-cell circulation pattern, the direction of motion shows the warm air rising at the equator ($\theta = \frac{\pi}{2}$) and falling at the pole ($\theta = 0$). In this case, the temperature deviation T is the difference between the temperature of a particular latitude and $-q\cos 2\theta$ (see equation 2.2.13). With gap width $R = 3.4$ and heating parameter $q = 0.0017$, the solutions of this model as presented in Figure 4.1(2nd row) are qualitatively the same, without any obvious difference, as the ones presented in Figure 4.1(1st row). For the same heating parameter q, the gap width R and rotation rate Ω in both solutions, a single-cell circulation pattern is observed that reaches from the equator to the pole.

Also in [11, 10], as the heating parameter q increases, there is a transition from a

single-cell circulation pattern to a triple-cell circulation pattern. This form of transition to multiple cells is also observed in our model. The solution of the radiative forcing model is as shown in Figure 4.2(2nd row) and is compared with the similar solution of [10] in Figure 4.2(1st row), for the corresponding parameter values.

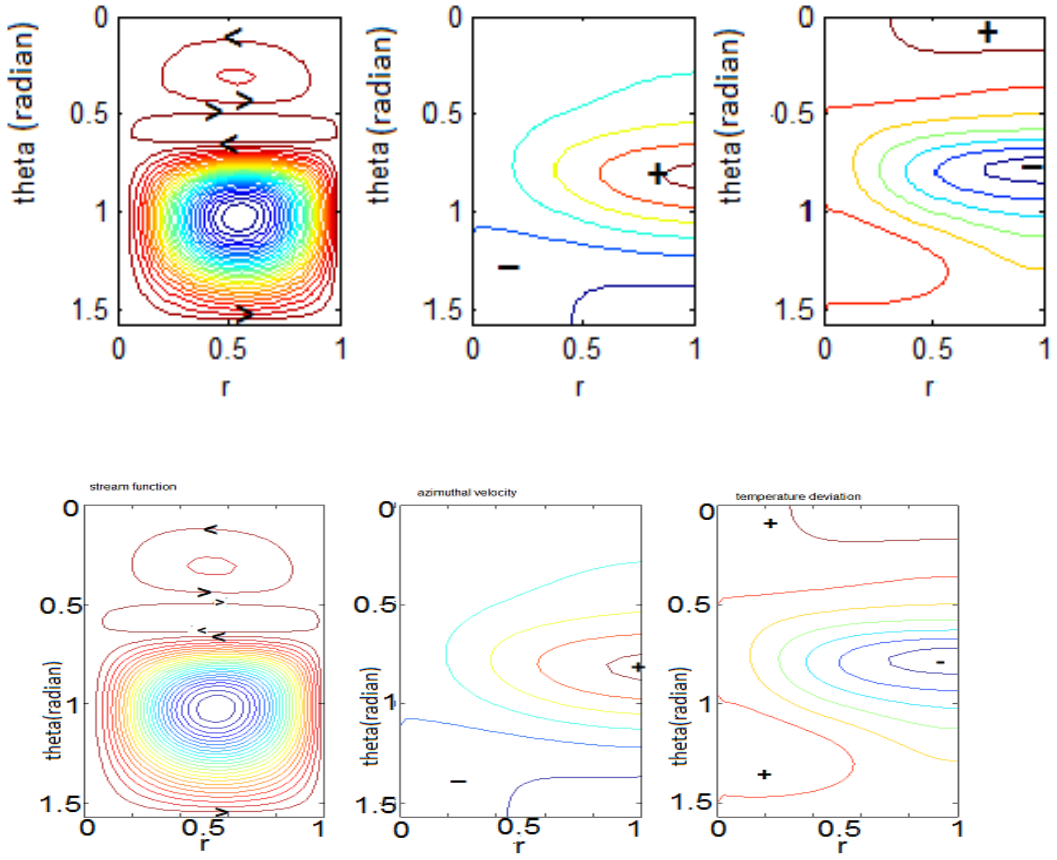

Figure 4.2: (1st row): Taken from the model of [10] with stress-free on outer boundary: A three-cell circulation pattern observed for heating parameter $\Delta T = 0.0037$. (2nd row): A three-cell circulation pattern observed for heating parameter $q = 0.0037$, gap width $R = 3.4$, rotation rate $\Omega = 0.01$ and with parameters chosen to mimic prescribed temperature on the inner boundary. From left to right, the stream function ξ; the azimuthal velocity u and the temperature deviation T from $-q\cos 2\theta$ on the inner boundary.

The three cells observed here are similar to the earth's convective cells, i.e. the Hadley, the Ferrel and the polar cells, respectively (see Section 1.1.4). The Hadley cell is observed in the tropics, the polar cell at the polar latitudes, and the Ferrel cell in between the Hadley cell and the polar cell. A significant difference is that the

earth's Hadley cell is bounded between the equator and 30^0 latitude in both northern and southern hemispheres. While in our solution, the first cell (i.e. the Hadley cell) from the equator reaches well beyond 30^0 latitude. This extension of our Hadley cell, alters the relative latitudinal positions of the other two cells when compared one to one with the corresponding convective cells of the earth. Nevertheless, they share many qualitative features. The azimuthal velocity u also exhibits similarity with atmospheric flow. For example, the jet stream is a westerly (i.e. blowing from the west) strong wind appearing in the mid-latitudes and having maximum velocity near the top of the tropopause. The trade winds are predominantly easterly (i.e. blowing from the east) appearing in the tropics. The similarity is easily explained. Take the northern hemisphere of the earth, for instance. The earth rotates in a counter-clockwise direction. The fluid that moves from the polar region towards the equator will get deflected to the right, and its direction of motion (easterly) will contradict that of the earth (westerly). This is indicated with a '$-$' sign in Figure 4.2, and it corresponds to the trade winds. Also, the fluid that moves from the equator towards the pole will have the same direction of motion (westerly) as the rotation of the earth. This is indicated with a '$+$' sign in Figure 4.2, and it corresponds to the jet stream. The jet stream is observed in the mid-latitudes while the trade wind is observed in the tropics. The difference is the polar westerly winds that are absent in our results.

Figure 4.3(2nd row) are the stream functions for different values of the heating parameter q, for the radiative forcing model, while Figure 4.3(1st row), are the stream functions for the case of the model in [10], with prescribed temperature on the inner boundary. The temperature deviation from the reference profile (i.e. $T_r - q\cos 2\theta$) at the boundary, is shown in Figure 4.4 for both cases of prescribed temperature and the radiative forcing. It is obvious from Figure 4.4 that the prescribed temperature case fixes the deviation of temperature from reference profile of each latitude to zero, and this coincides with the reference temperature $T_r = 0$. The radiative forcing allows each latitude to respond to forcing differently. However, the response of the latitude to changes in temperature does not appear to have a significant effect on the flow patterns, although it appears to allow transition to multiple cells at a slightly smaller

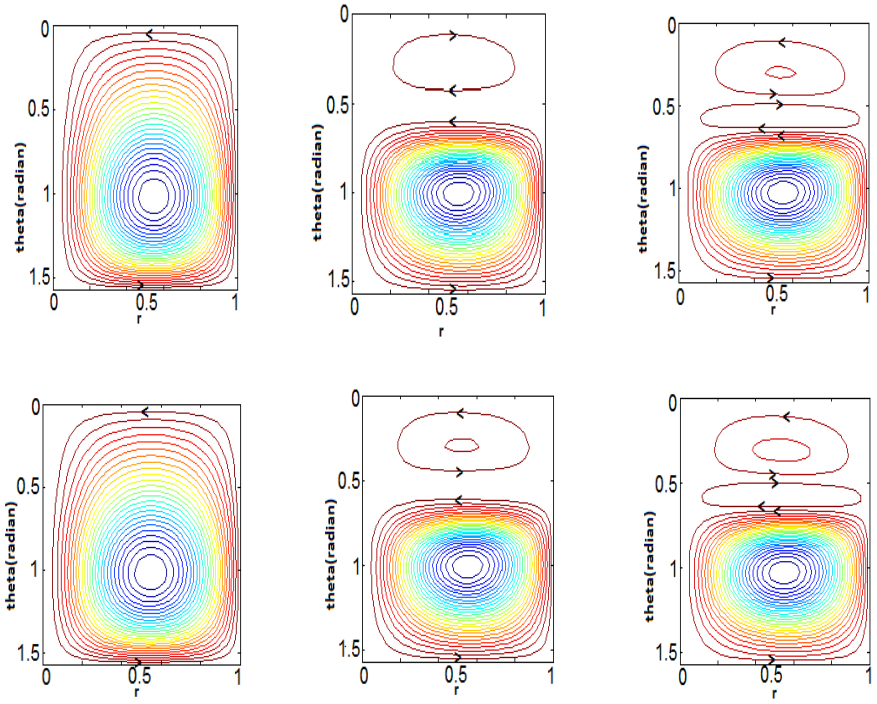

Figure 4.3: A sequence of transition from one to multiple circulation patterns observed for different heating parameters. (1st row): Taken from the model of [10] with stress-free on outer boundary: (left to right) $\Delta T = 0.0010$, $\Delta T = 0.0030$ and $\Delta T = 0.0037$. (2nd row): with radiative forcing and parameter values in Table 4.1: (left to right) $q = 0.0010$, $q = 0.0030$ and $q = 0.0037$, with gap width $R = 3.4$ and rotation rate $\Omega = 0.01$. The figures show only the stream function plots

value of q.

The mode of transition to multiple circulation cells in both cases described above are similar. It is observed that when $q = 0$, there is nothing happening in the system, but for small and nonzero q, there is a convective cell that reaches from the equator to the pole. A further increase in q causes the single cell to start shrinking towards the equator, until a new convective cell is formed next to the pole. These two convective cells are found to have the same flow orientation. This is made possible because of a gap between the two convective cells in which the flow is stationary. It is known that two convective cells with the same flow orientation can not be next to each other without such a gap in between them [14, 11, 10]. If the differential heating is increased further, the two cells adjust for the formation of the third convective cell. The third

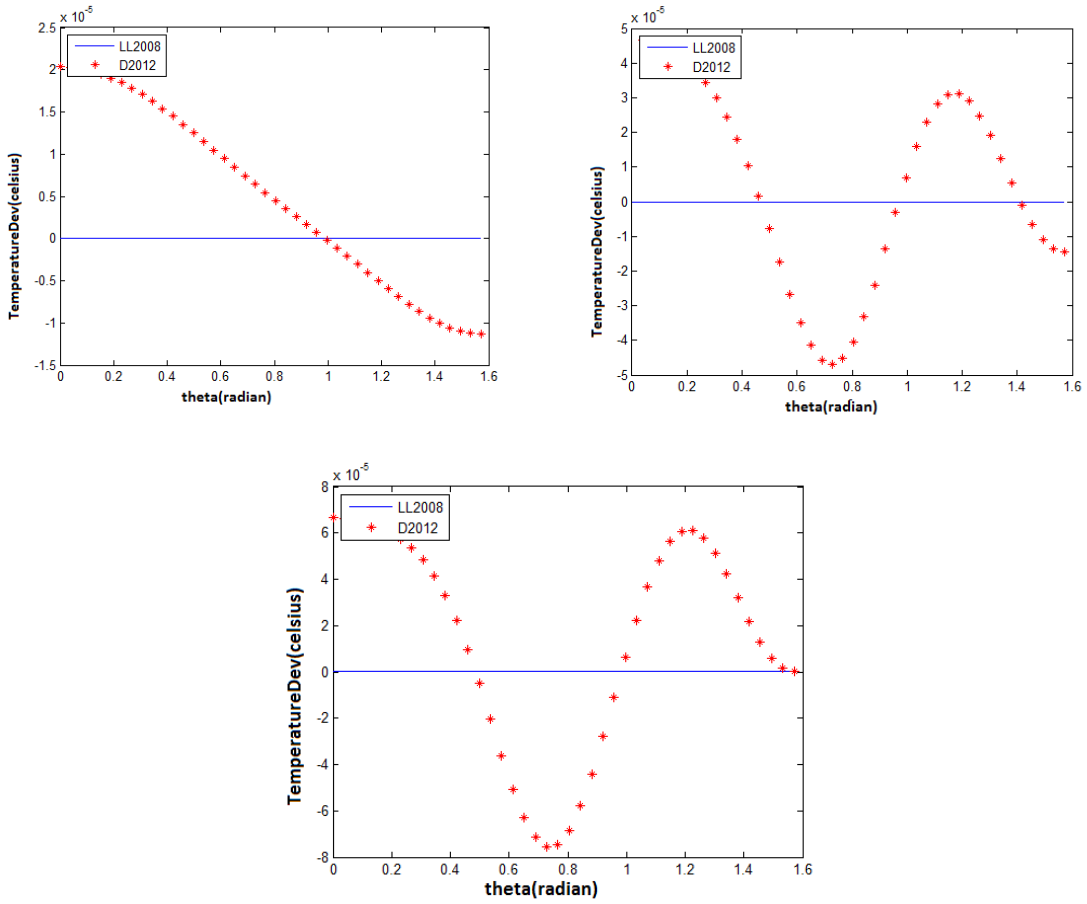

Figure 4.4: The comparison of temperature deviation on the inner boundary for radiative forcing and prescribed temperature for $q = 0.0010$, $q = 0.0030$ and $q = 0.0037$ respectively. The blue straight line is the reference temperature $T_r = 0$.

cell forms in between the two existing cells, and has contrary flow orientation. The convective cells for different values of the differential heating are qualitatively the same for both cases of prescribed temperature and radiative forcing, as the ones shown in Figures 4.2 and 4.1. Although both prescribed temperature and radiative forcing cases give qualitatively the same flow patterns as is evident in Figure 4.3, it seems that in the radiative forcing model, a small value of the differential heating is required to induce the transition to multiple cells.

4.2 Effects of Lower Boundary Conditions on Transitions

In this section, we solve the radiative forcing model with stress-free boundary conditions on the fluid velocity on the inner spherical shell, while keeping all parameter

values (see Table 4.1) the same, as in the case of the model with no-slip boundary conditions on the inner spherical shell. The observed difference in patterns of circulation due to this change in boundary condition is as shown in Figure 4.5. The heating

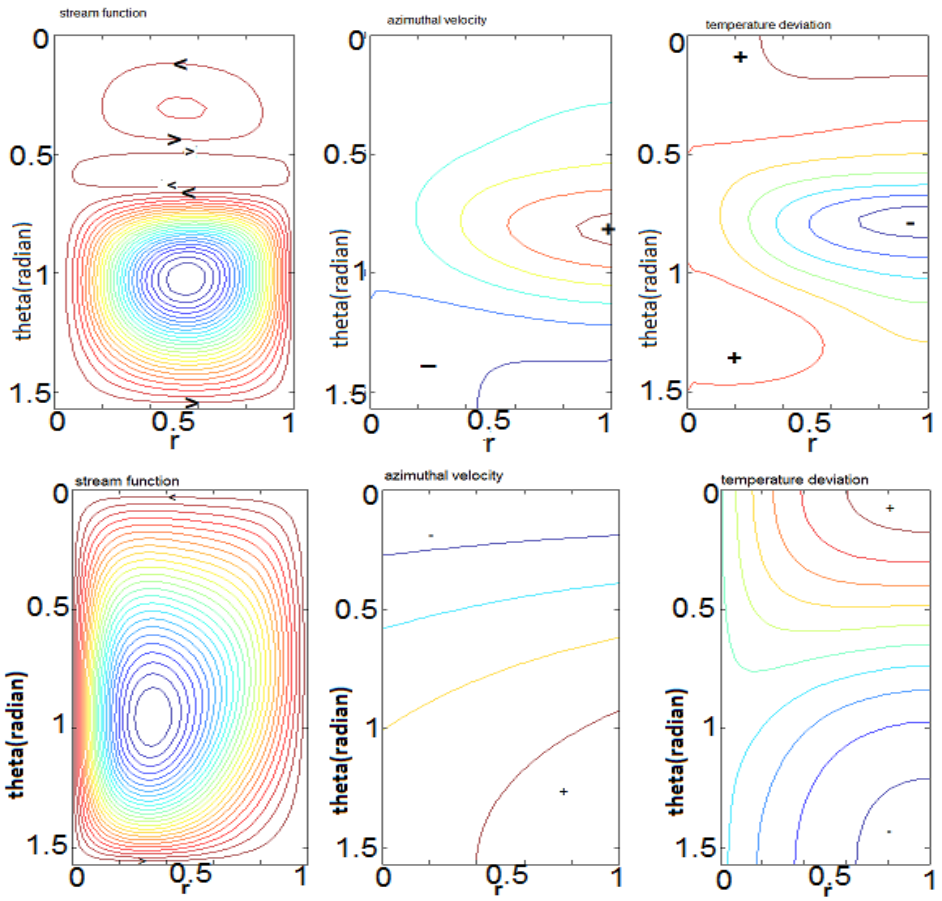

Figure 4.5: (1st row): With no-slip boundary conditions. (2nd row): With stress-free boundary conditions.

parameter q is allowed to increase from $q = 0$ to $q = 0.0037$ in both cases, and it is observed that with no-slip boundary conditions, there is a transition from a one-cell to a three-cell circulation pattern. This form of transition is not observed for values of heating parameter $0 \leq q \leq 0.0037$ in the system with stress-free boundary conditions. Furthermore, in the stress-free case, when the heating parameter q is increased further to $q = 0.0147$, the convective cell remains qualitatively the same without any form of transition to multiple convective cells. That is, there is still only one cell. Thus, it appears that the no-slip boundary condition plays a fundamental role in the transi-

tion. At the very least, it enables the transition to occur at a much smaller value of differential heating q than in the stress-free case. This is discussed further in Section 4.5.

In similar works on rotating spherical shells, where transition to multiple convective cells occurs, the transition is associated with a bifurcation [14, 11]. Therefore, in the next section, we only search for bifurcation in the radiative forcing model, with no-slip inner boundary conditions on velocity.

4.3 Hysteresis and Multiple Transitions

In this section, we discuss hysteresis and transition to multiple cells, in order to understand the possible link between the two. Hysteresis can occur when a real eigenvalue of a system crosses the imaginary axis (i.e. changes from negative to positive) and it changes back to negative by crossing the imaginary axis a second time. At each crossing of the eigenvalue, a saddle-node bifurcation occurs and the solution curve turns back on itself. This creates an S-shaped curve, where there is a region in parameter space in which three steady solutions exist simultaneously. The transition as presented in Section 4.1 has no such crossing of the eigenvalue and so no region of multiple steady solution exits. It was shown in [11], however, that as a second parameter, specifically the gap width, is varied the transition can become hysteretic. The point in parameter space at which this occurs is called a *cusp point* or *cusp bifurcation*.

In our search for hysteresis, we shall substitute the importance of Reynolds number in [13, 14] with differential heating, because the forcing for our radiative model is not from the rotation rate of the inner sphere, but from differential heating as in [11, 10]. We choose to discuss the hysteresis and the transition to multiple cells in terms of the aspect ratio $\eta = \frac{r_a}{r_b}$, where $r_b = r_a + R$, and the differential heating parameter q. Also, we redefine the radius ratio $r_R = \frac{R}{r_a}$, where $R = r_b - r_a$ is the gap width, and r_b is the radius of the outer shell, as in [11], in terms of aspect ratio η. Thus, we have $r_R = \frac{1-\eta}{\eta}$. Also, we define the set of critical values of the aspect ratio and differential heating, at which transition to multiple cells occurs, as (η_t, q_t). Similarly, we define the set of critical values of the aspect ratio and differential heating, at which a cusp bifurcation

occurs, as (η_c, q_c).

The following reasoning is relevant because it points to the fact that there could be some instances where hysteresis can occur without being accompanied by transition from single to multiple cells. In [11], with aspect ratio of $\eta_t = 2.9$ and differential heating $q_t = 0.0037$, there is transition from one to three convective cells, but at the critical points $\eta_c = 0.426$ and $q_c = 0.020$, where the cusp bifurcation that is associated with the transition occurs, there is transition from one to two convective cells. There are two crucial points to note here. One, it takes more heating to initiate transition at lower aspect ratio. Two, if the cusp bifurcation had occur at some critical point $\eta_c = 0.426$ and q, such that $q \leq q_t$, the hysteresis observed may not be accompanied by transition from one to multiple convective cells because of the point mentioned above.

The transition to multiple convective cells in the radiative forcing model, with $(\eta_t, q_t) = (2.9, 0.0037)$, is as shown in Figure 4.5. The associated maximum real eigenvalues, for both cases of no-slip and stress-free, are shown in Figure 4.6. None of the maximum real eigenvalues is zero or positive. The search for hysteresis requires one to carefully follow the behavior of the eigenvalues of the system for different combinations of (η, q). Figure 4.7 shows the convective cell, along with the azimuthal velocity and temperature deviation from $-q\cos 2\theta$, for $(\eta, q) = (0.5, 0.001)$. The single convective cell is not unexpected, because the differential heating $q = 0.001$ is such that $q < q_t$ with a smaller aspect ratio $\eta < \eta_t$. Therefore, the differential heating q can not initiate transition to multiple convective cells in the geometry with $\eta = 0.5$. The behavior of the maximum real eigenvalues in Figure 4.7 is similar to what is observed in [11] for the same aspect ratio (although the combination of radii is different: $R = 12$ and $r_a = 12$ and the differential heating value is different: $q = 0.020$). A further decrease in the aspect ratio from $\eta = 0.5$ to $\eta_c = 0.22$ clearly reveals the maximum eigenvalues of the system crossing the imaginary axis and returning again. This behavior of the maximum real eigenvalues is what is required for hysteresis as mentioned above. Figure 4.10 shows the maximum real eigenvalues crossing the imaginary axis and the continuation of the steady solution, turning upon itself twice,

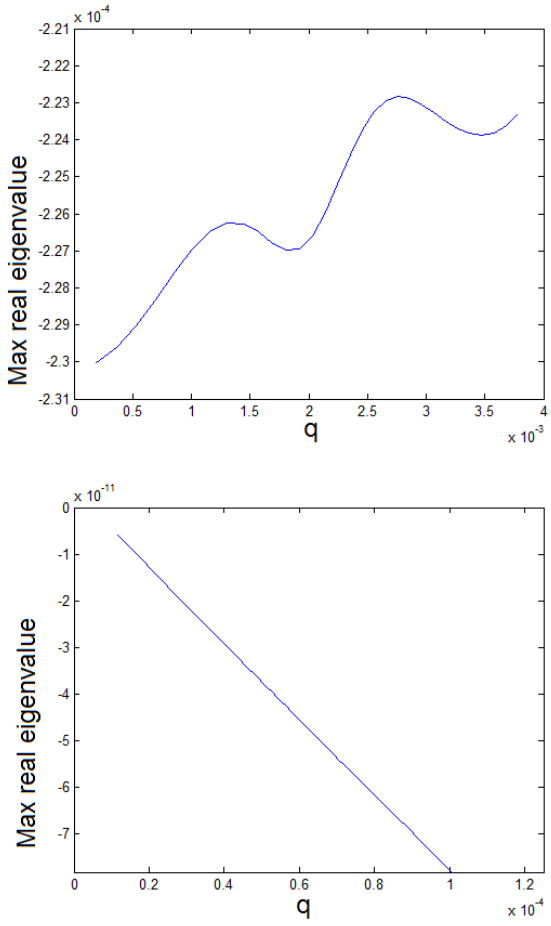

Figure 4.6: Up to Down: The maximum real eigenvalue of no-slip boundary system and maximum eigenvalue of stress-free boundary system.

thereby forming an S-shaped curve. The continuation of the steady solution shows two turning points. The portion of the solution before and after the turning points corresponds to the negative eigenvalues of the system, and they are said to be *linearly stable*. In fact, for those values of the differential heating q_c for which they both exist, they are said to be *bistable*. The portion of the solution between the two turning points corresponds to the positive values of the eigenvalues, and the corresponding solution is *linearly unstable*. Figure 4.9 shows the associated convective cell, the azimuthal velocity and the temperature deviation from $-q\cos 2\theta$. Again, the single cell is as expected because we are dealing with lower aspect ratio and low differential heating value $q_c = 0.001$, such that $q_c < q_t$. For further discussion, see Section 4.5.

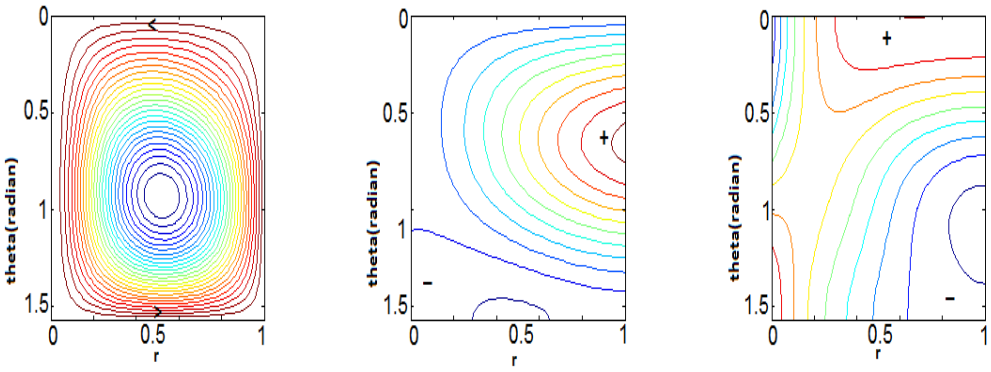

Figure 4.7: From left to right: A single convective cell, the azimuthal velocity and the temperature deviation for $q = 0.001$, $R = 3$, $r_a = 3$ and aspect ratio $\eta = 0.5$.

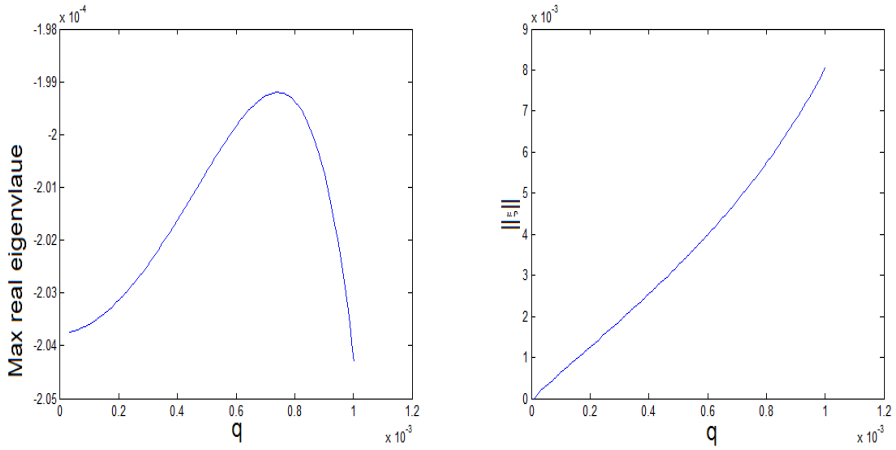

Figure 4.8: The plot of maximum real eigenvalues and continuation of steady solution for $R = 3$, $r_a = 3$ and aspect ratio $\eta = 0.5$.

4.4 Some Results Relevant to Climate

For the sake of the application of some of the results to our present-day climate, the differential heating is chosen as $q = 0.0037$ (this value is chosen because at the differential heating $q = 0.0037$, there are three convective cells). Though q is the differential heating for the system, it has a direct relationship with actual solar constant Q as described in Chapter 2. Specifically, the corresponding value of the solar constant for the chosen value of differential heating q is $Q = 0.028$. The actual value of the solar constant for the earth is $Q = 0.14$, which corresponds to $q = 0.018$. In this section, we study the response of each latitude to a change in the heating. This response is

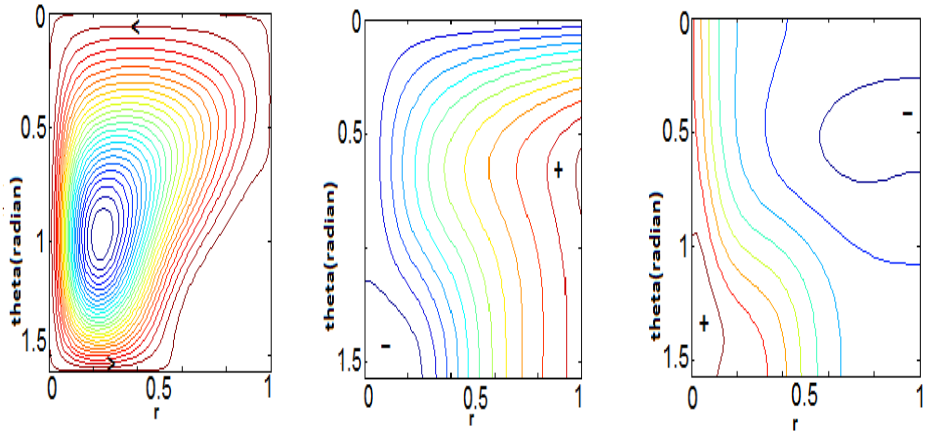

Figure 4.9: From left to right: A single convective cell, the azimuthal velocity and the temperature deviation from $-q\cos 2\theta$ for $q_c = 0.001$, $R = 10.50$, $r_a = 3$ and aspect ratio $\eta_c = 0.22$.

presented in each figure in terms of the temperature deviation from the reference profile (i.e. $T_r - q\cos 2\theta$). The 'normal' solar amount is the assumed present-day amount of solar radiation energy $q = 0.0037$, and any form of alteration to the normal solar amount is called 'shifted'.

4.4.1 Temperature Deviation and Circulation Pattern

The azimuthally and annually averaged atmospheric circulation on the earth consists of three convective cells, the Hadley, the Ferrel and the polar cells. Both Hadley and polar cells have the same direction of circulation but the Ferrel cell has contrary circulation direction. It is observed in this study that there is a correlation between the direction of motion of each cell, and the response of the temperature deviation from reference profile at the latitudes in which it exists. In each of the figures, a straight line is drawn tangent to the temperature deviation from the reference profile curve at the equator, and it is extended to the pole, such that each of the regions enclosed by the curve above the line is assigned '+' sign and those below the line is assigned a '−' sign. In Figure 4.11, the quantity of heat is low, and we have a single cell. The '+' sign indicates that there is a single circulation cell, that will rise and fall at the equator and pole respectively.

As the heating parameter increases, even before the transition from one cell to

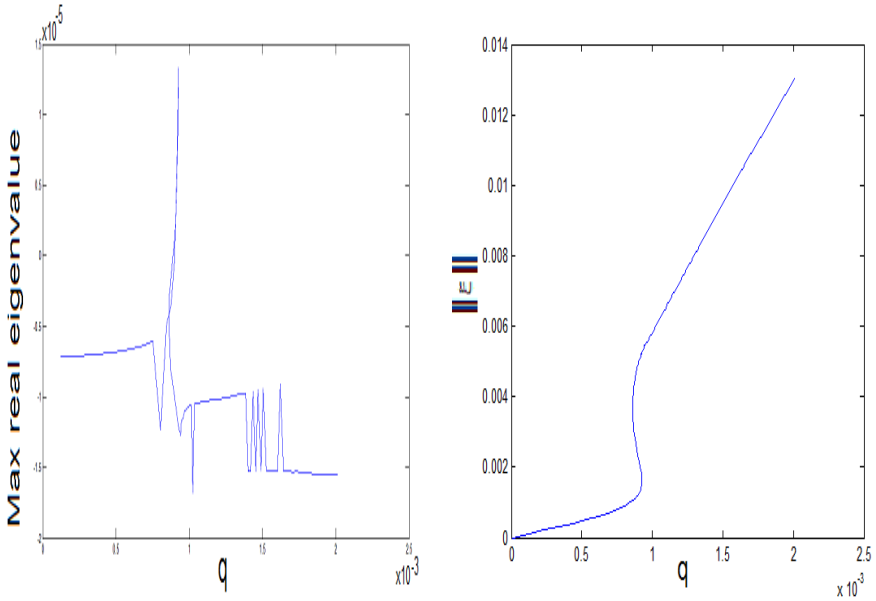

Figure 4.10: The plot of maximum real eigenvalues and continuation of steady solution for $R = 10.50$, $r_a = 3$ and aspect ratio $\eta_c = 0.22$.

two cells, there is a form of contrary temperature deviation in the mid-latitudes as shown in Figure 4.12, separating the two '+' signs. This implies that the two cells that will eventually form can have the same direction of circulation, with the cell at the pole having the same direction of circulation as the cell at the equator. It is worth mentioning that, an existing cell will not change its orientation, irrespective of the number of new cells that is formed. At its birth, the second cell circulates as the first cell as shown in Figure 4.13.

Further increase in heating leads to transition from two cells to three cells, with the third cell occupying the position made ready for it between the first and second cells. The figure depicting this is shown in Figure 4.14. It is also observed that this form of contrary temperature deviation happens when there is a transition from an odd number of cells to an even number of cells. The position and direction of circulation for subsequent cells will follow the same pattern. It is of interest to test the validity of this observation. The heating is increased further until there is a transition from three cells to four cells, and the result is as shown in Figure 4.15. All the odd-numbered cells have the same circulation direction and all the even-numbered cells

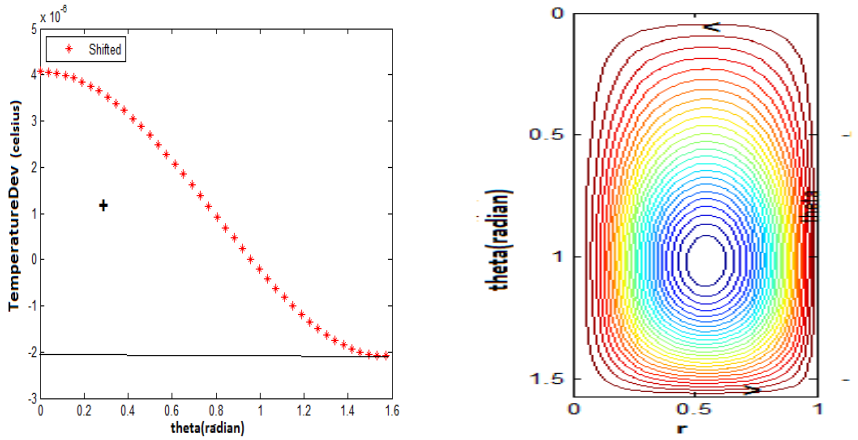

Figure 4.11: Right: A one-cell pattern with $q = 0.001$. Left: The curve is the temperature deviation from reference profile. Table 4.1 shows values for computation with $\Omega = 0.01$ and $R = 3.4$. The straight line is drawn tangent to the curve at the equator.

have the same circulation direction which is opposite to that of the odd-numbered cells.

4.4.2 The Effects of Solar Radiation on Mean Temperature

We define T_0 to be the annually averaged temperature at which a permanent ice sheet forms. That is, it is assumed that all latitudes for which $T < T_0$ will be ice-covered. Thus, assume that, for a given amount of incoming solar radiation $q_i = q_0$, where $q_0 = 0.0037$, the ice sheet is present for all colatitudes $\theta < \theta_i$. Now if there is a decrease in the amount of incoming solar energy q_i, there is a tendency for the ice boundary θ_i to shift equator-wards, due to a temperature decrease. Figure 4.16 shows the case of solar constant being reduced by about 10% (i.e. $q_i = 0.9q_0$) and $T_0 = 1\text{x}10^{-4}$. The pole ($\theta = 0$) exhibits more drop in temperature than the equator ($\theta = \frac{\pi}{2}$). It is also observed that there is an overall drop in mean temperature. If the solar amount is increased by 10% (i.e. $q_i = 1.10q_0$) and $T_0 = 1\text{x}10^{-4}$, there is a proportionate increase in the mean temperature of the earth. Figure 4.17 shows the increased (or 'shifted') heat energy against the 'normal' heat energy (i.e. $q_i = q_0$). Though there is an overall temperature increase, the polar temperature responds lesser than that of the equator. So, comparing both cases of reduced and increased solar energy, it is obvious that the equatorial region is more sensitive to a change in incoming solar radiation.

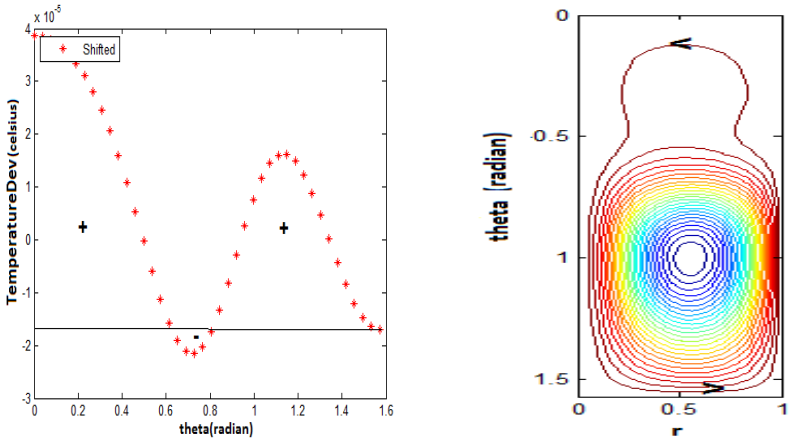

Figure 4.12: Right: A one-cell pattern with $q = 0.0025$. Left: The curve is the temperature deviation from the reference profile. Table 4.1 shows values for computation with $\Omega = 0.01$ and $R = 3.4$. The straight line is drawn tangent to the curve at the equator.

4.4.3 Effects of Ice Boundary on Mean Temperature

Figure 4.18 presents the cases for which the temperature of the ice boundary T_0 is changed from $T_0 = 1^0C$ to $T_0 = 0^0C$. The figure shows that an ice-covered planet will result from a reduction in annually-averaged temperature of the earth and an ice-free planet will result from an increased annually-averaged temperature. This is not unexpected and it confirms the effectiveness of the ice-albedo feedback mechanism incorporated into the radiative forcing equation via the Hill function. Moving the ice boundary temperature from $T_0 = 0^0C$ to $T_0 = 1^0C$, shows a drop in temperature distribution, and this corresponds to an ice-covered planet. Figure 4.18(1st row) shows that the response at the pole is maximum for ice-covered planet and minimum for ice-free planet. There seems to be an indication that the pole is more sensitive to heating in an ice-covered planet than the equator, and reverse seems to be the case in an ice-free planet.

4.4.4 Sensitivity of Latitudes to a Change in the Heating

Global warming is a phenomenon that comes with increased heating of the atmosphere. This leads to increasing average temperature of the earth, to the ice boundary moving towards to the pole, and to a melting of the ice sheet. In this section, we seek to

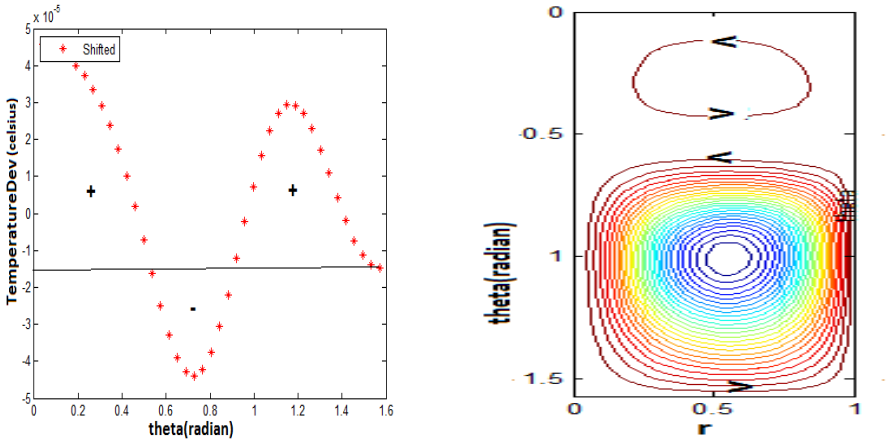

Figure 4.13: Right: A two-cell pattern with $q = 0.0030$. Left: The curve is the temperature deviation from the reference profile. Table 4.1 shows values for computation with $\Omega = 0.01$ and $R = 3.4$. The straight line is drawn tangent to the curve at the equator.

understand how vulnerable the ice is to a change in the heating. In Figure 4.19, it is assumed that the temperature deviation of the present-day climate follows the *middle* curve, and thus the increased heating follows the *upper* curve and the reduced heating follows the *lower* curve. Specifically, let q_N be the heating for the normal solar radiation, q_R for the reduced solar heating and q_I for the increased solar heating. Let $q_N = 0.0037$, $q_I = 1.10q_N$ and $q_R = 0.9q_N$, where q_I and q_R are 'shifted' solar amounts. The temperature deviation is taken from the earth's surface and the extreme points of the pole and equator are considered in computing the values in Table 4.2. We define, $\Delta Inc. = T_I - T_N$ and $\Delta Dec. = T_R - T_N$, where T_N is the temperature deviation from reference profile at normal solar heating, T_R at reduced solar heating, and T_I at increased solar heating.

Latitude	Normal	Inc.(^0C)	Dec.(^0C)	Δ Inc. x10^{-3}(^0C)	Δ Dec.x10^{-3}(^0C)
Pole	0.0106	0.0119	0.0085	1.3000	-2.1000
Equator	0.0111	0.0124	0.0089	1.3000	-2.2000
Temp. Gradient	0.0005	0.0005	0.0004		

Table 4.2: The response of the pole and equator to changes in solar heating. Table 4.1 shows values for computation with $\Omega = 0.01$, $D_R = 0$, $R = 3.4$ and $T_0 = 1\text{x}10^{-4}$.

From the result shown in Figure 4.19 and Table 4.2, we may infer that the equa-

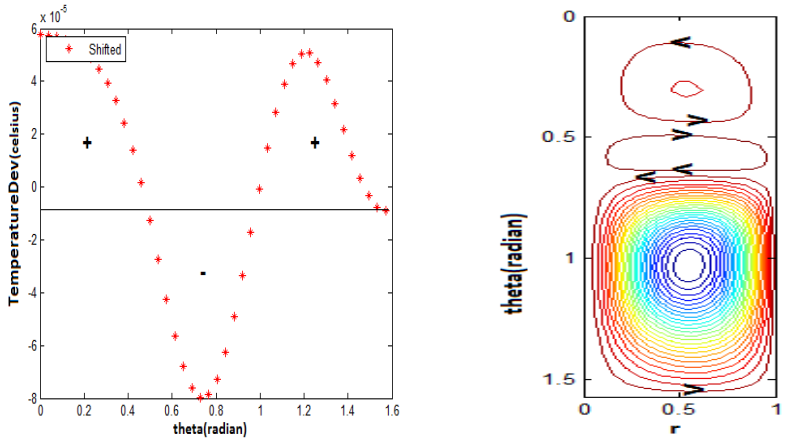

Figure 4.14: Right: A three-cell pattern with $q = 0.0037$. Left: The curve is the temperature deviation from the reference temperature. Table 4.1 shows values for computation with $\Omega = 0.01$ and $R = 3.4$. The straight line is drawn tangent to the curve at the equator.

torial latitudes are more sensitive to reduced heating than the polar latitudes, while they both respond equally to increased heating. The interpretation of Table 4.2 is as follows. We shall consider the entries of the table in terms of their absolute values. If we reduce the heating until we have an ice-covered planet, that is, if we reduce q until the temperature at the equator is $T_0 = 1\text{x}10^{-4}$, then the ice boundary will be at the equator. Similarly, if we increase the solar heating until we have an ice-free planet, i.e. such that the ice boundary is at the pole, then the polar temperature will be $T_0 = 1\text{x}10^{-4}$. Table 4.2 shows that with the same quantity of change in heating, the equatorial latitudes respond more to an increase in heating than the polar latitudes respond to a reduction in heating. This equatorial sensitivity could suggest that, it may take more change in heating to have an ice-free planet than is required to have an ice-covered planet. This opinion agrees with Sellers that stated that a 2%-5% decrease in solar radiation could initiate an ice-aged regime and an increase of 3%-10% could be needed to have an ice-free earth [22]. The difference may be connected with the curvature of the earth, in particular with the increase in the slope associated with the change in solar heating $S(\theta)$ as a function of latitude.

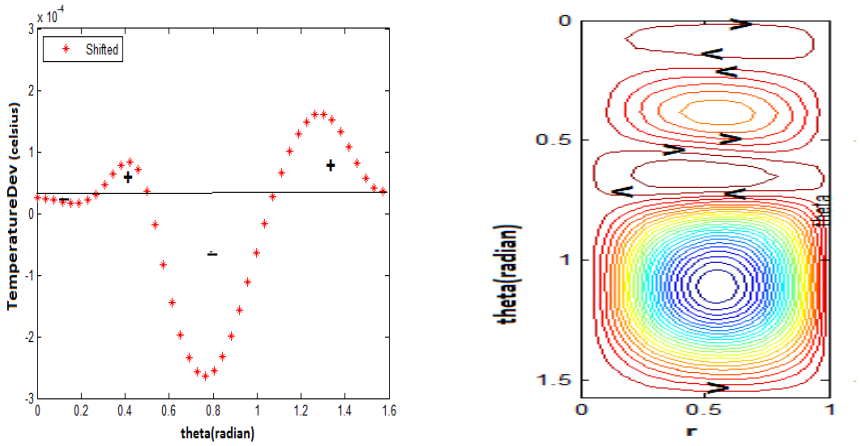

Figure 4.15: Right: A four-cell pattern with $q = 0.0070$. Left: The curve is the temperature deviation from the reference temperature. Table 4.1 shows values for computation with $\Omega = 0.01$ and $R = 3.4$. The straight line is drawn tangent to the curve at the equator.

4.5 Discussions

There will always be convection in a differentially heated spherical shell, with either radiative forcing or prescribed temperature on the inner boundary of the shell. For as long as there is differential heating in the system, no matter how small the quantity of heating might be, or the nature of boundary condition that is imposed on velocity on the inner boundary of the spherical shell, there will be onset of convection. The differential heating could be seen as being responsible for driving the system dynamics coupled with the boundary conditions. As shown in Figure 4.1, for a small quantity of heating, the convection appears as a single cell extending from equator to pole. This pattern of motion may remain the same for a large range of values of the heating parameter, or it may change, depending on the nature of the lower boundary condition imposed on the system's velocity.

The boundary layer or viscosity effect may be necessary to have transition from one cell to multiple cells. Modeling the problem with stress-free boundary conditions on the inner boundary switches off the effect of the friction between the boundary layer of the fluid and the inner boundary. Consequently, there is a significant reduction in energy dissipation at the boundary, and the fluid has much more energy to rise at the equator and travel far to the polar area before falling. By comparing the circulation

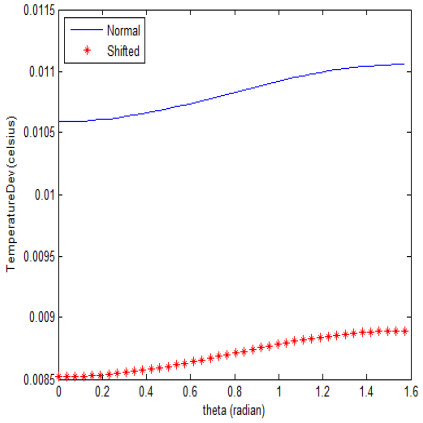

Figure 4.16: The response of each latitude to a change in the heating: temperature deviation is plotted as a function of colatitude θ for the case of reduced solar amount. The upper curve is for the 'normal' solar amount $q_i = q_0 = 0.0037$ and the lower curve is for the reduced solar amount $q_i = 0.9q_0$. There is an overall reduction in temperature deviation. Table 4.1 shows values for computation with $\Omega = 0.01$, $D_R = 0$, $R = 3.4$ and $T_0 = 1\text{x}10^{-4}$.

patterns in Figures 4.5(1st row) and 4.5(2nd row), it is obvious that in the no-slip case the fluid that rises at the equator does not go far to the pole before falling, and the other two convective cells build up between it and the pole. This could be due to the fact that the fluid that is rising at the equator area has lost some energy as a result of friction at the boundary layer, and in the single cell configuration the fluid is unable to balance the pressure gradient between the equator and the pole, set up by the increased differential heating.

As shown in Section 4.4.1, we find a correlation between the temperature deviation from reference profile on the inner surface and the flow orientation of the convective cells. The direction of motion of a cell at a particular latitude seems to be greatly influenced by the response of the latitude to a change in heating. Also, if we have more than three convective cells, the correlation is still maintained.

The transition to multiple convective cells that is observed in the model with radiative forcing is similar to the one observed in [11, 10], in which the transition to multiple cells is attributed to a cusp bifurcation. The transition to multiple convective cells is not dependent on the type of forcing that drives the system. Marcus *et al.* [13,

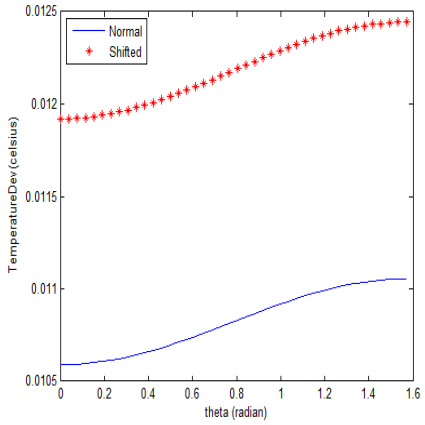

Figure 4.17: The response of each latitude to a change in the heating: temperature deviation is plotted as a function of colatitude θ for the case of increased solar amount. The lower curve is for the 'normal' solar amount $q_i = q_0 = 0.0037$ and the upper curve is for the increased solar amount $q_i = 1.10q_0$. There is an overall increment in temperature deviation. Table 4.1 shows values for computation with $\Omega = 0.01$, $D_R = 0$, $R = 3.4$ and $T_0 = 1\text{x}10^{-4}$.

14] used rotation rate of the inner boundary of the spherical shell, to drive the model they studied, Lewis and Langford [11, 10] used differential heating with prescribed temperature on the inner boundary of the spherical shell to drive their model, and radiative forcing on the inner boundary of the spherical shell is used in our model. In all the above cases, there are transitions to multiple convective cells. If the cusp bifurcation attributable to the transition occurs in the spherical shell with small aspect ratio, with the quantity of differential heating that is not sufficient to cause transition to multiple cells in a large aspect ratio, the corresponding hysteresis may not be accompanied by transition to multiple convective cells. It is also observed that more heating is required to initiate transition to multiple convective cells in a spherical shell with small aspect ratio.

The three cell circulation pattern so obtained in this study is similar to what is observed on present-day planet earth. Despite the similarity, they are not totally identical to the Hadley, the Ferrel and the Polar cells. The convective cell at the equator in our model goes beyond 30^0 of the equator, therefore, it alters the positions of the other two cells. Regardless, it is still reasonable to relate some of our results with

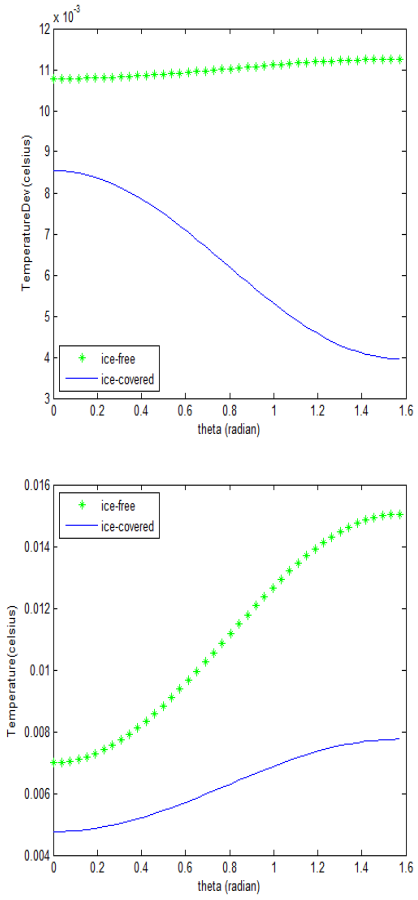

Figure 4.18: (1st row) The plot of temperature deviation from reference profile for $T_0 = 0^0C$(green), corresponds to an ice-free planet, and $T_0 = 1^0C$(blue) corresponds to an ice-covered planet. (2nd row) The plot of temperature distribution for both cases of $T_0 = 0^0C$(green) and $T_0 = 1^0C$(blue). Table 4.1 shows values for computation with $q = 0.0037$, $\Omega = 0.01$, $D_R = 0$ and $R = 3.4$. The temperature deviation and temperature distribution are plotted as a function of colatitude θ.

the earth's atmospheric conditions. It is known that the climatic condition at the mid-latitudes is always under the influence of the extreme climatic conditions at the polar latitudes and the equatorial latitudes. This combined contrary climatic conditions could be responsible for the response of the mid-latitudes to a change in heating as shown in Subsection 4.4.1. To bridge the gap between the two extreme conditions, the convective cell in the mid-latitudes have a circulation pattern that serves as a conveyor belt between the two.

The sensitivity of each latitude to a change in heating is put to test in Subsection 4.4.4. From the assumed present-day climate situation, the amount of heating that is

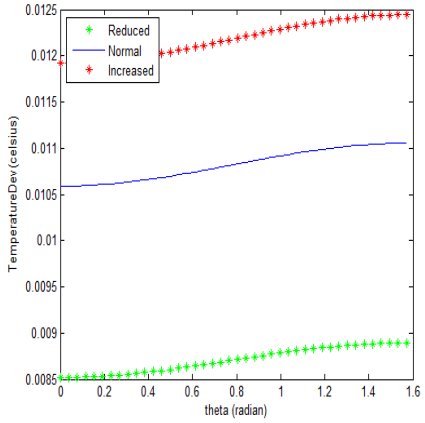

Figure 4.19: Sensitivity of each latitude to change in the heating: the case of normal (*middle curve*), reduced (*lower curve*) and increased (*upper curve*) solar heating. Table 4.1 shows values for computation with $\Omega = 0.01$, $D_R = 0$, $R = 3.4$ and $T_0 = 1\text{x}10^{-4}$. The temperature deviation is plotted as a function of colatitude θ.

available for the dynamics of the atmosphere is changed i.e. increased and decreased, by the same percentage, while keeping the temperature of the ice boundary constant. It is observed that the equator responds more to a decrease in heating than the pole, while they respond the same way to increased heating. It could be inferred from this latitudinal behavior that the ice-covered planet might be easier to achieve than ice-free planet. Finally, from Figure 4.18(1st row) there seems to be an indication that in an ice-covered planet, the pole may respond more to heating than the equator and this response is reversed for an ice-free planet.

Chapter 5
Conclusion and Future Work

5.1 Conclusion

The transition to multiple convective cells is robust in a differentially heated rotating spherical shell of Bousinessq fluid, provided a no-slip condition is imposed on the velocity at the inner boundary. This transition to multiple convective cells may be attributed to hysteresis. In other words, hysteresis is necessary for transition to multiple convective cells in a differentially heated co-rotating spherical shell of Bousinessq fluid. This may not be true for all systems with spherical shell geometry, where there is transition to multiple convective cells [13, 14]. In a system of differential heated co-rotating spherical shell of Bousinessq fluid, where there are transition to multiple cells and hysteresis, the transition is usually found in the spherical shell with large aspect ratio, while the hysteresis that is associated with it will usually be found in the spherical shell with small aspect ratio. Nevertheless, the hysteresis may or may not be accompanied by transition to multiple cells, if the aspect ratio is small and the quantity of differential heating is also small. The occurrence or non-occurrence of the transition along with the hysteresis phenomenon depends on the value of the heating parameter at which the hysteresis occurs. For a small differential heating value that is not sufficient to initiate transition to multiple cells in a spherical shell with large aspect ratio, the hysteresis that occurs at that heating value may not be accompanied by transition to multiple cells.

The current discussion in meteorology is about global warming, which is a consequence of the atmosphere not being transparent enough for outgoing long-wave radiation. With some technological advancements that could lead to increased carbon dioxide and other greenhouse gases in the atmosphere, these gases will continue to

restrict the outgoing radiation, by absorbing it and re-emitting it, to warm the atmosphere. Table 4.2 shows that the equator responds more to change in heating than the pole and this could imply further change in heating might lead to an ice-covered planet faster than ice-free planet. Also Figure 4.19 shows latitudinal response to change in heating. It could be inferred that, with global warming which leads to increased heating for the atmosphere, the ice boundary will continue to move pole-wards until all the ice is melted. The consequence of this ice-free regime in our planet can be grave, and it includes higher temperature. The increased average annual temperature will lead to the extension of desert areas and these areas will not be able to support the growth of most plants. Also, the melted ice will flow into the sea and the sea level will rise. The sea-level rise will cause rivers and oceans to overflow their banks leading to excessive flooding of many habitable places and farm vegetation. To maintain the presence of the ice-sheet, the atmosphere would have to retain its current level of transparency to the outgoing radiation; the human activities that increase the amount of greenhouse gases in the atmosphere would have to be reduced or controlled. On the other hand, if the amount of solar radiation for the heating of the atmosphere is somehow reduced, e.g. by excessive volcanic activity, then we might experience the ice boundary moving to the mid-latitude and possibly to the equator, depending on how reduced the heating might be.

Despite some understandings of the earth's climate we have derived from the solutions of this model, it has many limitations. The size of the geometry is negligibly small when compared to the size of the earth. As a result of this, the parameter values are different from those of the earth and the heating parameter for the model can not be increased to match the solar constant for the earth. Having said that, this laboratory-scale model and the earth are dynamically similar in terms of balance of forces and the boundary conditions as they affect the motions (i.e. transport processes).

5.2 Future Work

The future work on this project could include the ocean-atmosphere heat transfer mechanisms into the radiative forcing, as there is significant heat exchange between the ocean and the atmosphere. The ocean absorbs a significant amount of solar radiation because of its low albedo and acts as a heat sink. The absorbed radiation is converted to heat energy and is exchanged with the atmosphere, by various means; the significant medium of heat exchange with the atmosphere is through evaporation, because of the latent heat of vaporization of the water.

The solution of the model that breaks reflectional symmetry can be studied also. This will help to understand if the convective cells in northern hemisphere form before the ones in the southern hemisphere.

Bibliography

[1] M. Amabili. *Nonlinear Vibrations and Stability of Shells and Plates*. Cambridge University Press, New York, USA, 1st edition, 2008.

[2] O.P. Anders. Hadley′s principle: Understanding and misunderstanding the trade winds. *History of meteorology*, 3:17–42, 2006.

[3] G.B. Arfken and H.J. Weber. *Mathematical Methods for Physicists*. Elsevier Academic Press, 6th edition, 2005.

[4] M.I. Budyko. The effect of solar radiation variations on the climate of the Earth. *Tellus*, 21(5):611–619, 1969.

[5] W. Govaerts. Stable solvers and block elimination for bordered systems. *SIAM J. Matrix Anal. Appl.*, 12(3):469–483, 1991.

[6] W.J.F Govaerts. *Numerical Methods for Bifurcations of Dynamical Equilibria*. SIAM, Philadelphia, 1st edition, 2000.

[7] G. Hadley. Concerning the Cause of the General Trade Winds. *Phil. Trans. Roy. Soc.*, 39(436-444):58–62, 1735. `http://rstl.royalsocietypublishing.org/content/39/436-444/58.full.pdf+html`.

[8] E. Halley. An Historical Account of the Winds, and Monsoons, observable in the Seas between and near the Tropics, with an attempt to assign the Physical Cause of said Winds. *Phil. Trans. Roy. Soc.*, 16:153–168, 1686. `http://archive.org/details/philtrans09399630`.

[9] K. Kimura, S. Takehiro, and M. Yamada. Stability and bifurcation of Boussinesq thermal convection in a moderately rotating spherical shell. *American Institute of Physics*, 23(7):1–11, 2011.

[10] W. F. Langford and G.M. Lewis. Poleward expansion of Hadley cells. *Canadian Applied Mathematics Quarterly*, 17(1):105–119, 2009.

[11] G. M. Lewis and W.F. Langford. Hysteresis in a rotating differentially heated spherical shell of Boussinesq fluid. *SIAM J. Appl. Dyn. Sys.*, 7(4):1421–1444, 2008.

[12] J. Lu, G.A. Vecchi, and T. Reichler. Expansion of the Hadley cell under global warming. *Geophysical Research Letters*, 34, 2007. `http://www.agu.org/pubs/crossref/2007/2006GL028443.shtml`.

[13] P.S. Marcus and L.S. Tuckerman. Simulation of flow between concentric rotating spheres. Part 1. Steady states. *J. Fluid Mech.*, 185:1–30, 1987.

[14] P.S. Marcus and L.S. Tuckerman. Simulation of flow between concentric rotating spheres. Part 2. Transitions. *J. Fluid Mech.*, 185:31–65, 1987.

[15] United Nations. *United Nations Framework Convention on Climate Change*. United Nations, New York, 1992. `http://unfccc.int/key_documents/the_convention/items/2853.php`.

[16] M. Net, F. Garcia, and J. Sanchez. Numerical study of the onset of thermosolutal convection in rotating spherical shells. *American Institute of Physics*, 24(6):1–21, 2012.

[17] G.R. North. Theory of Energy-Balance Climate Models. *J. Atmos. Sci.*, 32(11):2033–2043, 1975.

[18] Intergovernmental Panel on Climate Change. *Climate Change 2007: Synthesis Report*. Intergovernmental Panel on Climate Change, Geneva, 2007. `http://www.ipcc.ch/publications_and_data/ar4/syr/en/contents.html`.

[19] P.B. Patil and U.P. Verma. *Numerical Computational Methods*. Alpha Science International Ltd., Oxford UK, 1st edition, 2006.

[20] J.P. Peixoto and A.H. Oort. *Physics of Climate*. American Institute of Physics, New York, 1st edition, 1992.

[21] R.T. Pierrehumbert. *Principles of Planetary Climate*. Cambridge University Press, 1st edition, 2010.

[22] W.D. Sellers. A global climate model based on the energy balance of the earth-atmosphere system. *J. Appl. Meteorol.*, 8(3):392–400, 1969.

[23] K. Zhang and X. Liao. A new asymptotic method for the analysis of convection in a rapidly rotating sphere. *J. Fluid Mech.*, 518:319–346, 2004.